Photoelectrochemical Solar Energy Conversion with Metal Nano-dotted and Surface-alkylated n-Type Silicon (n-Si) Electrodes

Susumu TAKABAYASHI

Division of Chemistry,

Department of Chemical Science and Engineering,

Graduate School of Engineering Science,

Osaka University

2005

Contents

General Introduction

The solar energy that is always streaming from the sun onto the earth has fostered all of us unconsciously for a long time. The nature has a great factory for solar energy utilization as the “photosynthesis” and its ingenious mechanism is now quite attractive from a scientific point of view. If the artificial utilization of the solar energy is realized as an energy resource, our life will become more and more pleasant and fertile. A main method of the artificial solar energy utilization is the photovoltaic conversion using solar cells because the electric energy is one of the most indispensable energies for our modern life. The photovoltaic conversion is also desired from another view-point of environment protection, because the thermal power generation by using fossil fuels, which is the main energy resources in the present societies, emits a large amount of CO_2 gas to cause the green house effect (global warming), together with NO_x and SO_x gases to cause environmental pollution. Furthermore, the fossil fuels are limited in amount on the earth and will have to be used in the best way under deep considerations.

Fortunately, recent progress in studies on single crystal silicon (Si) p-n junction solar cells has realized high conversion efficiencies close to the theoretical limit. Very high conversion efficiencies have also been achieved for tandem-type solar cells with MOCVD-made high-quality compound semiconductors. However, a serious problem has still remained in that the fabrication costs for these solar cells are quite high, about 10 times higher than the cost for practical application on large scales. Thus, the main target in the present solar-cell studies lies in lowering the fabrication cost without reducing the conversion efficiency.

One of the most promising approaches to this target is to develop high-efficiency thin-film solar cells, fabricated with inexpensive thin-film semiconductor materials. In fact,

much attention has recently been paid to this-type solar cells,[1-3] such as amorphous silicon (Si) solar cells, polycrystalline Si thin film solar cells, and dye-sensitized TiO_2 solar cells. However, we have to mention that this-type solar cells have faced a serious deadlock because the use of expensive transparent conductive oxide (TCO) such as indium tin oxide is inevitably necessary for efficient current collection. In addition, the TCO has no enough electrical conductivity and thus it is needed to adopt a complex solar-cell structure composed of series connection of a large number of tiny solar cells to avoid an increase in the current density and hence in the ohmic loss,[4] which leads to a significant cost increase. Furthermore, this series-connection structure induces another cost increase because high-quality fabrication of tiny solar cells is required, for in this structure damage of one tiny cell ruins all the performance of tiny cells connected in series with it.

Another promising approach is to develop an efficient and stable solar to chemical conversion system, such as solar water splitting, by use of a semiconductor/electrolyte junction.[5] Merits of this approach lie in that (1) inexpensive thin-film semiconductor materials can easily be used and (2) photogenerated electrons and holes are converted to chemical fuels such as hydrogen and oxygen within a photoelectrolysis cell and thus no current collection (and no TCO) is necessary.

The main problem in developing the direct solar to chemical conversion system lies in that it is difficult to find an efficient and stable semiconductor electrode. It is well known [6] that titanium dioxide (TiO_2) is stable and can oxidize water into oxygen and H^+ ions, but it only absorbs UV light and is inefficient in solar energy conversion.[7,8] On the other hand, a silicon (Si) semiconductor is one of the most suitable semiconductors for solar energy conversion in view of an appropriate band-gap of 1.1 eV for obtaining a high efficiency, abundance in natural resources, and non-toxicity.[9] However, Si has a serious problem when it is used as a photoelectrode in aqueous electrolytes, in that it is easily oxidized at the surface and

passivated.[10-23]

Recently, a number of studies have been reported on modification of Si surfaces with organic alkyl groups.[24-32] A large merit of surface alkylation is the improvement of Si stability against the surface oxidation in air[33] and in an aqueous redox electrolyte,[34] without any increase in the surface carrier recombination rate. However, it is also reported[34-40] that the surface alkylation tends to retard interfacial electron transfer at the Si/redox electrolyte contacts. The surface alkylation for the Si stabilization has thus faced a serious dilemma on this point.

On the other hand, the research group to which the author belongs has studied for a long time the metal nano-dot coating for obtaining efficient n-Si electrodes. The studies have revealed[23,41-47] that single crystal n-Si electrodes loaded with Pt nano-dots, in a Br^-/Br_2 aqueous redox electrolyte, generate very high open-circuit photovoltages (V_{oc}) of 0.62 - 0.64 V, considerably higher than those of conventional solid-state p-n junction Si solar cells. This finding has provided a new way to utilize Si for solar to chemical conversion, but unfortunately the n-Si electrode showed no enough stability for long-term operation. Theoretically, it was expected[41,42] that the Si surface was stabilized by metal particles at metal-coated parts and Si-oxide layers at naked parts, but actually gradual Si oxidation occurred even beneath the metal particles, which led to the electrode degradation.

Under these circumstances, the author started studies on the n-Si electrodes for the purpose of obtaining the high-efficiency and stable electrodes. The main strategy was to combine the method of surface alkylation for the stability and the method of metal nano-dot coating for the high efficiency. The author has finally succeeded in demonstrating that the surface alkylated and Pt nano-dotted n-Si electrodes are really the high-efficiency and stable electrodes. He has also succeeded in clarifying some important new aspects in the surface modification, in relation with the control of the flat-band potential as well as the method to

prepare doubly surface-modified electrodes such as the surface alkylated and Pt nano-dotted n-Si electrodes.

In the first chapter, it is shown that the surface methylation (CH_3-termination), combined with the Pt nano-dot coating, can provide an efficient and stable n-Si (111) electrode for use in a photoelectrochemical (PEC) cell. The surface methylated and Pt nano-dotted n-Si electrodes showed efficient and stable photocurrents in an aqueous HBr/Br_2 redox electrolyte of a highly corrosive nature for more than 6 h. It is also shown that the Pt nano-dots can act as an effective catalyst (or gates) for interfacial electron transfer, which effectively overcomes the demerit of the surface alkylation to retard the interfacial electron transfer.

In the second chapter, the properties of the surface methylated and Pt nano-dotted n-Si electrodes in an aqueous I_3^-/I^- redox electrolyte are studied in detail. This-type electrodes gave a high V_{oc} of about 0.57 V and the photovoltaic characteristics were stable for more than 24 h, in contrast to hydrogen (H)-terminated and Pt nano-dotted n-Si electrodes for which the V_{oc} was only 0.3 to 0.4V and the photocurrent degraded seriously in 24 h. In addition, the electrodes of this type could successfully be used for photodecomposition of hydrogen iodide into hydrogen and iodine in an electrochemical cell with no external bias, and yielded a solar to chemical conversion efficiency (ϕ^s_{chem}) of 7.4 %, which is the highest ever reported, apart from high values reported for MBE-made expensive high-quality composite multiplayer semiconductor electrodes such as p-n $Al_xGa_{1-x}As$/p-n Si/Pt[48] and p-n GaAs/p-$Ga_xIn_{1-x}P$/Pt.[49,50] The success is of great importance, in that it has opened a new way of cost lowering for solar energy conversion.

In the third chapter, the photovoltage and stability of the Pt nano-dotted and surface-alkylated n-Si (111) electrodes in the I^-/I_3^- redox electrolyte are studied as a function of the chain length of surface alkyl groups. Linear sweep voltammetry revealed that the overvoltage for the Pt deposition became larger with increasing the surface alkyl chain length,

i.e., in the order of H-, CH_3-, *n*-C_4H_9-, and *n*-C_6H_{13}-, most probably because of decreased stabilization of surface ionic intermediate(s) of the Pt electrodeposition. SEM inspection and chronoamperometry revealed that the Pt particle density decreased and the particle size increased with increasing the alkyl chain length, suggesting that long alkyl chains attached to the n-Si surface lay down on it and covered non-alkylated sites at which the Pt deposition occurred, thus having a detrimental effect on the Pt deposition on n-Si. The photovoltaic behavior and stability for the surface alkylated n-Si were improved much by the Pt-dot coating, but became somewhat inferior with increasing the alkyl chain length, in harmony with the above model.

In the fourth chapter, the flat-band potentials (U_{fb}) for the Pt nano-dotted and surface alkylated n-Si (111) electrodes in the I^-/I_3^- redox electrolytes are studied in relation with their solar cell characteristics. It is found that the U_{fb} for the surface methylated and Pt nano-dotted n-Si (111) electrodes shifted toward the negative with increasing the I^- concentration, in parallel to the equilibrium redox potential $U_{eq}(I^-/I_3^-)$, and thus the V_{oc} was kept nearly constant among the redox electrolytes with different $U_{eq}(I^-/I_3^-)$ and different pH. This U_{fb} shift is explained by assuming that Si-I bonds are formed at a part of the n-Si surface to which no alkyl group nor Pt are attached and that adsorption of an I^- ion occurs at this bond in the form of Si-I···I^-, thus the induced negative surface charge causing the negative shift in U_{fb}. It is also shown from the measurements of the U_{fb} in the dark and under illumination that Pt dots really act as an efficient catalyst (gates or channels) for the interfacial electron transfer and prevents the positive shift in the U_{fb} under illumination.

References

(1) Chopra, K. L.; Paulson, P. D.; Dutta, V. *Prog. Photovolt.* **2004**, *12*, 69.

(2) Goetzberger, A.; Hebling, C.; Schock, H. W. *Mater. Sci. Eng., R* **2003**, *40*, 1.

(3) Shah, A.; Torres, P.; Tscharner, R.; Wyrsch, N.; Keppner, H. *Science* **1999**, *285*, 692.

(4) Yamamoto, K.; Yoshimi, M.; Tawada, Y.; Fukuda, S.; Sawada, T.; Meguro, T.; Takata, H.; Suezaki, T.; Koi, Y.; Hayashi, K.; Suzuki, T.; Ichikawa, M.; Nakajima, A. *Sol. Energy Mater. Sol. Cells* **2002**, *74*, 449.

(5) Tryk, D. A.; Fujishima, A.; Honda, K. *Electrochim. Acta* **2000**, *45*, 2363.

(6) Fujishima, A.; Honda, K. *Nature* **1972**, *238*, 37.

(7) Fujishima, A.; Kohayakawa, K.; Honda, K. *Bull. Chem. Soc. Jpn.* **1975**, *48*, 1041.

(8) Fujishima, A.; Kohayakawa, K.; Honda, K. *J. Electrochem. Soc.* **1975**, *122*, 1487.

(9) Sze, S. M. *Semiconductor Devices: Physics and Technology*, 2nd. ed.; John Wiley & Sons: New York, 2002.

(10) Nakato, Y.; Ohnishi, T.; Tsubomura, H. *Chem. Lett.* **1975**, 883.

(11) Nakato, Y.; Abe, K.; Tsubomura, H. *Ber. Bunsen-Ges. Phys. Chem.* **1976**, *80*, 1002.

(12) Kohl, P. A.; Frank, S. N.; Bard, A. J. *J. Electrochem. Soc.* **1977**, *124*, 225.

(13) Bolts, J. M.; Bocarsly, A. B.; Palazzotto, M. C.; Walton, E. G.; Lewis, N. S.; Wrighton, M. S. *J. Am. Chem. Soc.* **1979**, *101*, 1378.

(14) Bocarsly, A. B.; Walton, E. G.; Wrighton, M. S. *J. Am. Chem. Soc.* **1980**, *102*, 3390.

(15) Yoneyama, H.; Murao, Y.; Tamura, H. *J. Electroanal. Chem.* **1980**, *108*, 87.

(16) Noufi, R.; Frank, A. J.; Nozik, A. J. *J. Am. Chem. Soc.* **1981**, *103*, 1849.

(17) Fan, F. R. F.; Wheeler, B. L.; Bard, A. J.; Noufi, R. N. *J. Electrochem. Soc.* **1981**, *128*, 2042.

(18) Fan, F. R. F.; Hope, G. A.; Bard, A. J. *J. Electrochem. Soc.* **1982**, *129*, 1647.

(19) Skotheim, T.; Lundstroem, I.; Prejza, J. *J. Electrochem. Soc.* **1981**, *128*, 1625.

(20) Skotheim, T.; Lundstroem, I.; Delahoy, A. E.; Kampas, F. J.; Vanier, P. E. *Appl. Phys. Lett.* **1982**,

40, 281.

(21) Leempoel, P.; Castroacuna, M.; Fan, F. R. F.; Bard, A. J. *J. Phys. Chem.* **1982**, *86*, 1396.

(22) Rosenblum, M. D.; Lewis, N. S. *J. Phys. Chem.* **1984**, *88*, 3103.

(23) Nakato, Y.; Yano, H.; Tsubomura, H. *Chem. Lett.* **1986**, 987.

(24) Linford, M. R.; Chidsey, C. E. D. *J. Am. Chem. Soc.* **1993**, *115*, 12631.

(25) Linford, M. R.; Fenter, P.; Eisenberger, P. M.; Chidsey, C. E. D. *J. Am. Chem. Soc.* **1995**, *117*, 3145.

(26) Bansal, A.; Li, X. L.; Lauermann, I.; Lewis, N. S.; Yi, S. I.; Weinberg, W. H. *J. Am. Chem. Soc.* **1996**, *118*, 7225.

(27) Sung, M. M.; Kluth, G. J.; Yauw, O. W.; Maboudian, R. *Langmuir* **1997**, *13*, 6164.

(28) Buriak, J. M. *Chem. Commun.* **1999**, 1051.

(29) Cicero, R. L.; Linford, M. R.; Chidsey, C. E. D. *Langmuir* **2000**, *16*, 5688.

(30) Okubo, T.; Tsuchiya, H.; Sadakata, M.; Yasuda, T.; Tanaka, K. *Appl. Surf. Sci.* **2001**, *171*, 252.

(31) Buriak, J. M. *Chem. Rev.* **2002**, *102*, 1271.

(32) Wayner, D. D. M.; Wolkow, R. A. *J. Chem. Soc., Perkin Trans. 2* **2002**, 23.

(33) Royea, W. J.; Juang, A.; Lewis, N. S. *Appl. Phys. Lett.* **2000**, *77*, 1988.

(34) Bansal, A.; Lewis, N. S. *J. Phys. Chem. B* **1998**, *102*, 4058.

(35) Bansal, A.; Lewis, N. S. *J. Phys. Chem. B* **1998**, *102*, 1067.

(36) Yu, H. Z.; Boukherroub, R.; Morin, S.; Wayner, D. D. M. *Electrochem. Commun.* **2000**, *2*, 562.

(37) Barrelet, C. J.; Robinson, D. B.; Cheng, J.; Hunt, T. P.; Quate, C. F.; Chidsey, C. E. D. *Langmuir* **2001**, *17*, 3460.

(38) Cheng, J.; Robinson, D. B.; Cicero, R. L.; Eberspacher, T.; Barrelet, C. J.; Chidsey, C. E. D. *J. Phys. Chem. B* **2001**, *105*, 10900.

(39) Zhao, J. W.; Uosaki, K. *Appl. Phys. Lett.* **2003**, *83*, 2034.

(40) Niwa, D.; Inoue, T.; Fukunaga, H.; Akasaka, T.; Yamada, T.; Homma, T.; Osaka, T. *Chem. Lett.*

2004, *33*, 284.

(41) Nakato, Y.; Ueda, K.; Yano, H.; Tsubomura, H. *J. Phys. Chem.* **1988**, *92*, 2316.

(42) Nakato, Y.; Tsubomura, H. *Electrochim. Acta* **1992**, *37*, 897.

(43) Yae, S.; Nakanishi, I.; Nakato, Y.; Toshima, N.; Mori, H. *J. Electrochem. Soc.* **1994**, *141*, 3077.

(44) Nakato, Y.; Kai, K.; Kawabe, K. *Sol. Energy Mater. Sol. Cells* **1995**, *37*, 323.

(45) Kawakami, K.; Fujii, T.; Yae, S.; Nakato, Y. *J. Phys. Chem. B* **1997**, *101*, 4508.

(46) Jia, J. G.; Fujitani, M.; Yae, S.; Nakato, Y. *Electrochim. Acta* **1997**, *42*, 431.

(47) Ishida, M.; Morisawa, K.; Hinogami, R.; Jia, J. G.; Yae, S.; Nakato, Y. *Z. Phys. Chem.* **1999**, *212*, 99.

(48) Licht, S.; Wang, B.; Soga, T.; Umeno, M. *Appl. Phys. Lett.* **1999**, *74*, 4055.

(49) Khaselev, O.; Turner, J. A. *Science* **1998**, *280*, 425.

(50) Khaselev, O.; Turner, J. A. *Electrochem. Solid State Lett.* **1999**, *2*, 310.

Chapter 1

Stabilization of n-Si electrodes by Surface Alkylation and Metal Nano-Dot Coating for Use in Efficient Photoelectrochemical Solar Cells

Abstract

Surface methylated and Pt nano-dotted single crystal n-Si(111) electrodes yielded efficient photocurrent density (j) vs. potential (U) characteristics for more than 6 h in a highly corrosive electrolyte of aqueous 8.6 M HBr + 0.05 M Br_2. On the other hand, H-terminated and Pt nano-dotted n-Si electrodes degraded seriously in about 15 min. Surface methylated but non-Pt-dotted n-Si electrodes yielded only poor j-U characteristics with low V_{oc}. The results clearly show that a combination of surface alkylation and metal nano-dot coating is an effective way to obtain efficient and stable Si photoelectrodes and hence photoelectrochemical solar cells.

Introduction

The main target in recent studies on solar energy conversion is to realize a high-efficiency and low-cost solar conversion system in the form of either solar cells or solar water splitting. In particular, to realize a low-cost conversion system is of key importance in view of practical application on large scales. In this respect, thin film solar cells, made of inexpensive thin film semiconductor materials such as amorphous Si, polycrystalline Si, polycrystalline metal chalcogenides, and dye-sensitized nanocrystalline TiO_2 films, are a very promising approach, and much attention has been paid to this type of solar cells.[1]

The research group to which the author belongs reported previously[2-8] that single crystal (flat-surface) n-Si electrodes coated with metal nano-particles, in contact with a redox electrolyte such as 8.6 M HBr + 0.05 M Br_2, generated very high open-circuit photovoltages (V_{oc}) of 0.62 - 0.64 V, considerably higher than those of conventional solid-state p-n junction Si solar cells of a similar simple structure. This remarkable result is entirely due to a unique effect of metal nano-dot coating,[3,4] which leads to *ideal* semiconductor electrodes.[9] It should be emphasized that the method can be applied easily to inexpensive polycrystalline Si thin films. Also, solar cells of a solid-state type can be fabricated by the same principle.[6] However, this method still had a problem in that the n-Si electrodes did not show enough stability for long-tern operation.

Recently, a number of studies have been reported on the modification of Si surfaces with organic alkyl groups.[10-16] A large merit of surface alkylation is the improvement of Si stability against surface oxidation in air[17] and in an aqueous redox electrolyte,[18] without any increase in the surface carrier recombination rate.[17] However, it is also reported[19,20] that the surface alkylation tends to retard interfacial electron transfer at the Si/redox electrolyte contacts. In this chapter, the author reports that the surface alkylation, combined with metal nano-dot coating, can provide an efficient and stable n-Si electrode for use in photoelectrochemical solar cells. In

this approach, the metal nano-dots can act as an effective catalyst for interfacial electron transfer to overcome the demerit of the surface alkylation used for the Si stabilization.

Experimental

Single crystal n-Si (111) wafers of the resistivity of 1 ~ 5 Ω cm, donated by Shin-Etsu Handotai Co. Ltd., were used. The surfaces of the Si wafers were cleaned by washing in boiling acetone for 2 min and successive immersing in a mixture of 95% H_2SO_4 and 30 % H_2O_2 (1:1 in volume) at 100 °C for 20 min and in 5 % HF for 5 min. The hydrogen (H)-terminated Si surfaces were obtained by further consecutive immersion of the above Si wafer in a mixture of 25 % aqueous NH_3, 30 % H_2O_2, and water (1:1:5 in volume) at 80 °C for 20 min, in 5 % HF for 5 min, and in 40 % NH_4F for 15 min.

The alkylation (methylation) of the Si surface was, in this chapter, obtained by a method of photochlorination followed by Grignard reaction, which was first reported by Bansal et al.[12] An H-terminated n-Si (111) wafer was put in a saturated chlorobenzene solution of phosphorus pentachloride (PCl_5) and the solution was refluxed under UV illumination for 1 h. After washing with toluene, the wafer was put in a 3.0 M diethylether solution of CH_3MgI (Grignard reagent) and the solution was refluxed for 1 h. All the procedures were done under a dried argon atmosphere. The Si wafer thus methylated was finally washed with tetrahydrofuran and pure water.

Platinum nano-particles were deposited on the methylated Si surface by a method of dropping a Pt-colloid solution, which was prepared by the Bredig method.[4] Ohmic contact was obtained with indium-gallium alloy. The n-Si wafer thus prepared was then mounted in a Teflon holder (effective area: 0.25 cm^2) and used as an electrode in photoelectrochemical experiments.

Photocurrent density (j) vs. potential (U) was measured with a potentiostat (Hokuto-Denko HA 501) and a potential programmer (Nikko Keisoku NPS-2). A Pt plate was used as the counter electrode, and a saturated calomel electrode (SCE) was used as the reference electrode. Electrolyte solutions were prepared using special grade chemicals and

pure water, the latter of which was obtained from deionized water by purification with a Milli-Q water purification system. Surface inspection was carried out with a Hitachi S-5000 high-resolution scanning electron microscope (SEM). X-ray photoelectron spectroscopic (XPS) analysis was performed with a Shimadzu ESCA-1000 spectrometer using an MgKα line.

Results and Discussion

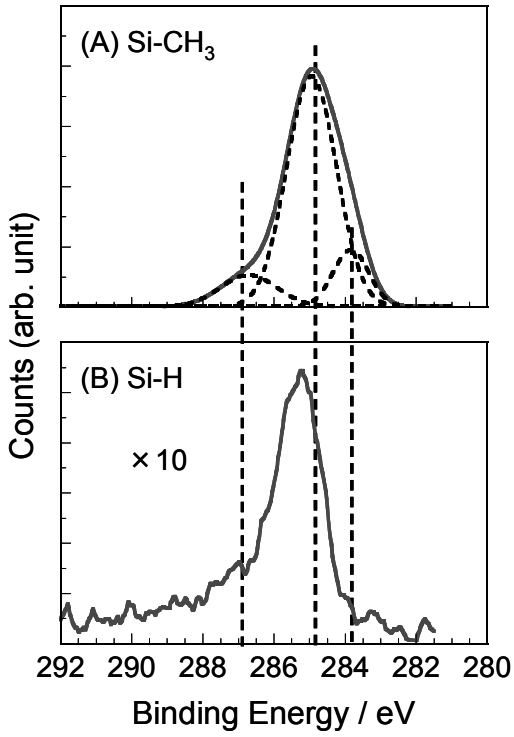

FIGURE 1 C-1s XPS peaks for (A) methylated (CH_3-terminated) and (B) hydrogen (H)-terminated Si surfaces. The broken lines in (A) are deconvoluted Gaussian curves for curve fitting.

The methylation of the n-Si surface by the above-described chemical treatment could be simply recognized with eyes by an increase in the hydrophobicity of the Si surface (or an increase in the contact angle for a water droplet at the Si surface). The methylation was also confirmed by XPS analysis. Figure 1 shows carbon-1s XPS peaks for (A) methylated (CH_3-terminated) and (B) hydrogen (H)-terminated Si surfaces. The main peak at about 284.9 eV, observed for both the Si surfaces, can be attributed to carbon in C-C bonds of contaminating hydrocarbons. A higher energy shoulder at about 286.7 eV can also be attributed to contaminating organic compounds, i.e., carbon of oxidized groups such as C=O in them. On

other hand, a lower energy shoulder at about 283.8 eV, which is only observed for the methylated (CH_3-terminated) Si surface, can be attributed to carbon in surface Si-CH_3 bonds. This assignment is in good agreement with the work reported by other workers.[15,21] Thus the author can conclude that the Si-CH_3 bonds are really formed at the n-Si surface in this chapter. A very rough estimation of the surface coverage (θ) of CH_3 group from the intensity of the 283.8-eV peak, with a correction for contributions of inside Si atoms by the method of Himpsel et al.,[22] led to a value of θ of around 70 %, which is somewhat higher than a reported value of less than 50 %[14] probably owing to an influence of contaminating organic compounds at the Si surface.

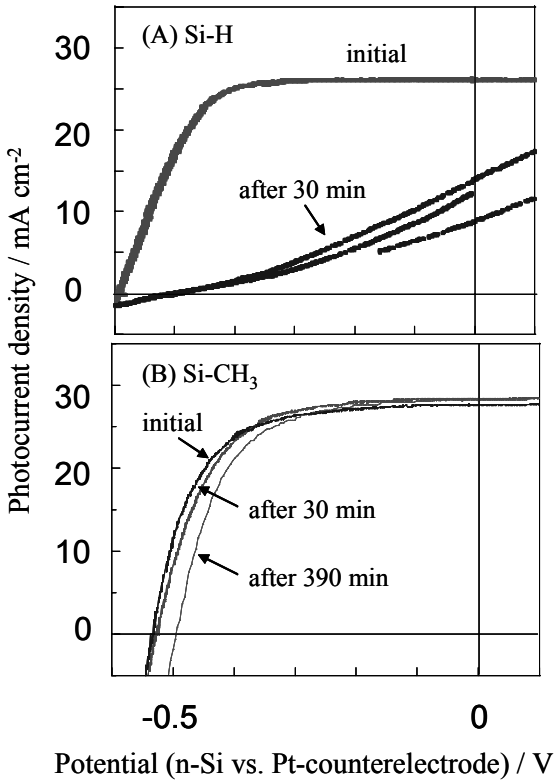

FIGURE 2 (A) A time course of the *j-U* curve for a non-methylated (H-terminated) and Pt nano-dotted n-Si electrode, and (B) that for a surface-methylated and Pt nano-dotted n-Si (111) electrode, both in 8.6 M HBr + 0.05 M Br_2 under continuous illumination by simulated solar light (AM 1.5G, 100 mW cm^{-2}).

Figure 2(B) shows a time course of photocurrent density (j) vs. potential (U) for a surface-methylated and Pt nano-dotted n-Si (111) electrode in a redox electrolyte of 8.6 M HBr + 0.05 M Br_2 under continuous illumination by simulated solar light (AM 1.5G, 100 mW cm^{-2}). For comparison, Figure 2(A) shows a time course of j vs. U for a non-methylated (H-terminated) and Pt nano-dotted n-Si electrode. The j-U curve for the methylated and Pt nano-dotted n-Si electrode remained unchanged, except a slight decrease in V_{oc}, under long-term continuous illumination for 390 min in a very corrosive solution of 8.6 M HBr + 0.05 M Br_2. On the other hand, the j-U curve for the H-terminated and Pt-nano-dotted n-Si electrode degraded seriously in 30 min (Figure 2A). The result clearly shows the effectiveness of the surface alkylation for obtaining stable n-Si electrodes.

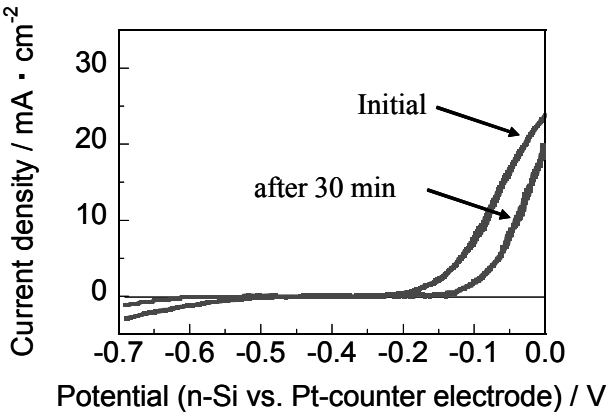

FIGURE 3 A time course of the j-U curve for a methylated but non-Pt-dotted n-Si electrode in 8.6 M HBr + 0.05 M Br_2 under continuous illumination by simulated solar light (AM 1.5G, 100 mW cm^{-2}).

It is to be mentioned here that methylated but non-Pt-dotted n-Si electrodes showed only poor j-U curves in 8.6 M HBr + 0.05 M Br_2, with the photocurrent onset at around –0.2 V, as shown in Figure 3, though H-terminated n-Si electrodes with no Pt showed fairly efficient j-U

curves at least at the very initial stage. This result indicates that the surface methyl group considerably retards the interfacial redox reaction. This conclusion is in contrast to the result of Bansal et al.,[18] who reported fairly efficient *j*-*U* curves for methylated n-Si in aqueous $[Fe(CN)_6]^{3-}/[Fe(CN)_6]^{4-}$. The difference may arise from the fact that the oxidation of $[Fe(CN)_6]^{4-}$ by photogenerated holes at the Si surface occurs by a simple electron transfer mechanism, treated by a Marcus-Gerischer theory, whereas the oxidation of Br^- occurs via adsorbed intermediate(s) at the electrode surface. It is likely that the surface methyl group hinders the adsorption of oxidized intermediates such as Br· atoms, which leads to the poor *j*-*U* curve for the methylated but no Pt dotted n-Si in aqueous Br^-/Br_2. The above argument clearly indicates the important role of metal nano-dot coating in obtaining efficient n-Si electrodes. In addition, it may be interesting to note that the poor *j*-*U* curve for the methylated but no Pt dotted n-Si electrode in aqueous Br^-/Br_2 was stable under continuous illumination for 30 min (Figure 3), contrary to the case of H-terminated n-Si with no Pt, again showing the effectiveness of the surface alkylation for the Si stabilization.

One may note from Figures 2A and 2B that the open-circuit photovoltage (V_{oc}) for the methylated and Pt-dotted n-Si electrode is, at the initial stage, slightly lower than that of the H-terminated and Pt-dotted one. Moreover, the V_{oc} for the methylated and Pt-dotted electrode decreases slightly with time under long-term illumination (Figure 2B), though the short-circuit photocurrent (j_{sc}) and the fill factor (*F.F.*) remains nearly unchanged. The fact that the *F.F.* remains unchanged strongly suggests that no surface oxidation proceeds in this case, for otherwise the *F.F.* should decrease to a large extent, as observed in Figure 2(A).

What is the reason for the decrease in the V_{oc} for the methylated and Pt-dotted electrode under long-term illumination? One possibility is to assume a change in the size and the separation of surface Pt particles during the illumination. The research group to which the author belongs reported before[3,4] that the optimal size and separation of surface Pt particles is

about 5 nm and about 200 nm, respectively. The increase in the size of the Pt particles, as well as the decrease in their separation, both lead to a decrease in the V_{oc} owing to a decrease in the barrier height for the n-Si/solution contact.[3,4]

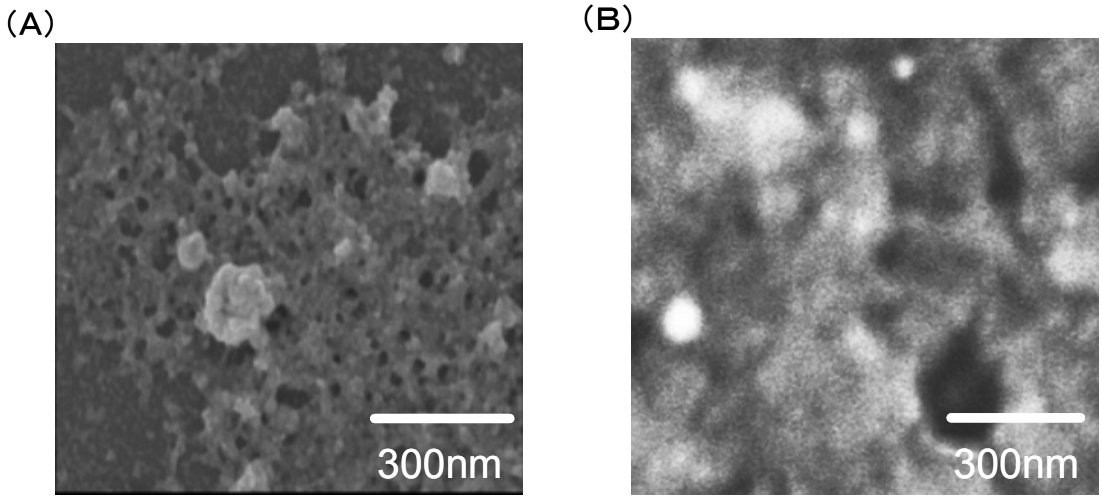

FIGURE 4 SEM images of surface-methylated and Pt-dotted n-Si (111) electrodes (A) before and (B) after a long-term stability test for 360 min.

Figure 4 shows SEM images of a surface-methylated and Pt-dotted n-Si (111) electrode (A) before and (B) after a long-term stability test for 360 min. Even at the initial stage, Pt particles exist as large aggregates (Figure 4A). Besides, the size of the Pt aggregates seems to increase after the long-term stability test, together with a change in the shape, though the image in (B) is blurred under best focused conditions for an unknown reason. The author might thus tentatively say that this increase in the size and the change in the shape (or the separation) of the Pt aggregates might be responsible for the decrease in the V_{oc} for the methylated and Pt nano-dotted Si electrode during the long-term stability test. It is likely that the Pt particles are photoanodically dissolved in 8.6 M HBr + 0.05 M Br_2 in the form of $PtBr_x$ to a slight extent under illumination, which leads to a change in the size and shape of the Pt aggregates during

long-term illumination.

It may be noted also that Pt particles exist as large aggregates even at the initial stage (Figure 4A), as already mentioned above. This may be the reason why the V_{oc} for the methylated and Pt-dotted n-Si electrode is, at the initial stage, lower than that for the H-terminated and Pt-dotted one (Figure 2). Such aggregation of the Pt particles arises from an experimental difficulty that the methylated Si surface is much more hydrophobic than the H-terminated one, and thus, when a Pt-colloid solution was dropped on the surface, the solution tends to form small round spheres. This necessitates us to drop a large amount of Pt-colloid solution to cover all over the Si surface. Anyway, further studies are necessary to get a definite conclusion on the reason for the decrease in the V_{oc} after the long-term stability test.

Why is the n-Si electrode stabilized by surface methylation? A possible explanation is that the surface methyl group forms a hydrophobic thin layer on the Si surface and prevents the approach of water molecules to it. At present the author have no information on the detailed morphological structures of surface methyl group and Pt particles and their interrelations on an atomic scale. More regulated alkylation and deposition of Pt particles are necessary to clarify these points. Such studies will be helpful for the improvement of the *j*-*U* characteristics and stability for the n-Si electrodes. A problem of slight degradation of *j*-*U* characteristics (Figure 2B), most probably arising from the aforementioned slight dissolution of Pt particles in the Br^-/Br_2 redox electrolyte, will be able to be overcome by choosing another appropriate redox couple. An interesting approach is to use the n-Si electrodes for solar water splitting in combination with another semiconductor electrode such as an N-doped (and hence visible-light absorbing) TiO_2 particulate film.

References

(1) Center for Photovoltaic Engineering, UNSW (The University of New South Wales) Home Page. http://www.pv.unsw.edu.au/Research/scet.asp (accessed Jan 2006).

(2) Nakato, Y.; Yano, H.; Tsubomura, H. *Chem. Lett.* **1986**, 987.

(3) Nakato, Y.; Ueda, K.; Yano, H.; Tsubomura, H. *J. Phys. Chem.* **1988**, *92*, 2316.

(4) Nakato, Y.; Tsubomura, H. *Electrochim. Acta* **1992**, *37*, 897.

(5) Yae, S.; Nakanishi, I.; Nakato, Y.; Toshima, N.; Mori, H. *J. Electrochem. Soc.* **1994**, *141*, 3077.

(6) Nakato, Y.; Kai, K.; Kawabe, K. *Sol. Energy Mater. Sol. Cells* **1995**, *37*, 323.

(7) Jia, J. G.; Fujitani, M.; Yae, S.; Nakato, Y. *Electrochim. Acta* **1997**, *42*, 431.

(8) Kawakami, K.; Fujii, T.; Yae, S.; Nakato, Y. *J. Phys. Chem. B* **1997**, *101*, 4508.

(9) Ishida, M.; Morisawa, K.; Hinogami, R.; Jia, J. G.; Yae, S.; Nakato, Y. *Z. Phys. Chem.* **1999**, *212*, 99.

(10) Linford, M. R.; Chidsey, C. E. D. *J. Am. Chem. Soc.* **1993**, *115*, 12631.

(11) Linford, M. R.; Fenter, P.; Eisenberger, P. M.; Chidsey, C. E. D. *J. Am. Chem. Soc.* **1995**, *117*, 3145.

(12) Bansal, A.; Li, X. L.; Lauermann, I.; Lewis, N. S.; Yi, S. I.; Weinberg, W. H. *J. Am. Chem. Soc.* **1996**, *118*, 7225.

(13) Sung, M. M.; Kluth, G. J.; Yauw, O. W.; Maboudian, R. *Langmuir* **1997**, *13*, 6164.

(14) Cicero, R. L.; Linford, M. R.; Chidsey, C. E. D. *Langmuir* **2000**, *16*, 5688.

(15) Okubo, T.; Tsuchiya, H.; Sadakata, M.; Yasuda, T.; Tanaka, K. *Appl. Surf. Sci.* **2001**, *171*, 252.

(16) Buriak, J. M. *Chem. Rev.* **2002**, *102*, 1271.

(17) Royea, W. J.; Juang, A.; Lewis, N. S. *Appl. Phys. Lett.* **2000**, *77*, 1988.

(18) Bansal, A.; Lewis, N. S. *J. Phys. Chem. B* **1998**, *102*, 4058.

(19) Cheng, J.; Robinson, D. B.; Cicero, R. L.; Eberspacher, T.; Barrelet, C. J.; Chidsey, C. E. D. *J. Phys. Chem. B* **2001**, *105*, 10900.

(20) Bansal, A.; Lewis, N. S. *J. Phys. Chem. B* **1998**, *102*, 1067.

(21) Terry, J.; Linford, M. R.; Wigren, C.; Cao, R. Y.; Pianetta, P.; Chidsey, C. E. D. *J. Appl. Phys.* **1999**, *85*, 213.

(22) Himpsel, F. J.; McFeely, F. R.; Talebibrahimi, A.; Yarmoff, J. A.; Hollinger, G. *Phys. Rev. B* **1988**, *38*, 6084.

Chapter 2

Efficient Solar to Chemical Conversion by a New-type n-Si Electrode with Metal Nano-contact and Surface Alkylation

Abstract

The author has succeeded in developing a new-type Si electrode with metal nano-contact and surface alkylation, which shows excellent and stable photovoltaic characteristics in aqueous redox electrolytes. The electrode has achieved solar decomposition of hydrogen iodide into hydrogen and iodine under no external bias with a solar to chemical conversion efficiency ϕ^{s}_{chem} of 7.4 %, which is the highest efficiency ever reported, apart from the values reported for high-quality expensive multilayer semiconductor electrodes. The present success is of great importance in that it has opened a new way of cost lowering for solar energy conversion.

Introduction

The main target in recent solar-cell studies lies in lowering the fabrication cost without reducing the conversion efficiency. Most attention has thus been paid to thin-film solar cells,[1,2] fabricated with inexpensive thin-film semiconductor materials such as amorphous silicon (Si), polycrystalline Si, and dye-sensitized TiO_2. However, this-type solar cells have faced a serious deadlock because the use of expensive transparent conductive oxide (TCO) such as indium tin oxide is inevitably necessary for efficient current collection. In addition, the TCO has no enough electrical conductivity and thus it is needed to adopt a complex solar-cell structure composed of series connection of a large number of tiny solar cells to avoid an increase in the current density and hence the ohmic loss,[2] which leads to a significant cost increase. Furthermore, this series-connection structure induces another cost increase because high-quality fabrication of tiny solar cells is required, for in this structure damage of one tiny cell ruins all the performance of tiny cells connected in series with it.

Solar to chemical conversion by use of a semiconductor/solution junction has attracted strong attention as another new technology for solar energy conversion, in particular, since the report of water splitting with n-TiO_2 in 1972 by Fujishima and Honda.[3] This method has great advantages in cost lowering over the thin-film solar cells, in that it does not use any expensive TCO and is easily adaptable to low-cost thin-film semiconductor materials. This method has, however, had the severe problem that most semiconductor electrodes with band-gaps suitable for solar energy conversion are chemically unstable in aqueous electrolytes.[4,5] For example, silicon (Si) is the most suitable semiconductor for solar energy conversion in view of an appropriate band-gap of 1.1 eV, abundance in natural resources, and non-toxicity, but easily oxidized and passivated in aqueous electrolytes. Stable semiconductors such as TiO_2, on the other hand, have wide band-gaps and absorb only UV light (or hardly absorb solar light). The dilemma has not been overcome for a long time.

The research group to which the author belongs reported fairly long ago[6-13] that single crystal n-Si electrodes loaded with metal nano-particles, immersed in a Br^-/Br_2 redox electrolyte, generated very high open-circuit photovoltages (V_{oc}) of 0.62 - 0.64 V, considerably higher than those of conventional solid-state p-n junction Si solar cells of a similar simple structure. This finding provided a new way to utilize Si for solar to chemical conversion, but unfortunately the n-Si electrode showed no enough stability for long-term operation. Theoretically, it was expected[7,8] that the Si surface was stabilized by metal particles at metal-coated parts and passivating Si-oxide layers at naked parts, but actually gradual Si oxidation occurred even beneath the metal particles, which led to the electrode degradation.

Recently, a number of studies have been reported on modification of Si surfaces with organic alkyl groups.[14-21] A large merit of surface alkylation is the improvement of Si stability against the surface oxidation in air[22] and in an aqueous redox electrolyte,[23] without any increase in the surface carrier recombination rate. However, it is also reported[24,25] that the surface alkylation tends to retard interfacial electron transfer at the Si/redox electrolyte contacts. The author reported in Chapter 1 that this problem could be solved by metal nano-dot coating because the metal nano-dots acted as an effective catalyst for interfacial electron transfer reactions.

The above finding is of great importance because it finally provides an effective way to utilize Si for solar to chemical conversion. In Chapter 1, the author studied the behavior of the n-Si electrode in 8.6 M HBr + 0.05 M Br_2 with a highly positive redox potential to get high V_{oc}'s. In this chapter, the author has studied the behavior of the n-Si in 7.6 M HI (or 7.6 M HI + 0.05 M I_2) to examine a possibility of efficient solar to chemical conversion via photodecomposition of HI into H_2 and I_2 (or I_3^-) with no external bias.

Experimental

Single crystal n-Si (111) wafers of the resistivity of 1 ~ 5 Ω cm and the thickness of 825 ± 25 μm, donated by New Win Go Co. Ltd., were used. The Si surfaces were cleaned by immersing in a boiling mixture of 95% H_2SO_4 and 30% H_2O_2 (3:1 in volume) for 15 min and in 5% HF for 5 min. The hydrogen (H)-terminated Si surfaces were obtained by further immersion in a boiling mixture of 25% aqueous NH_3, 30% H_2O_2, and water (1:1:5 in volume) for 15 min, followed by consecutive immersion in 5% HF for 5 min and 40% NH_4F for 15 min.

The alkylation (methylation) of the Si surface was obtained by a method of photochlorination followed by Grignard reaction, which was reported by Bansal et al.[16] and Okubo et al.[20] Namely, an H-terminated n-Si (111) wafer was put in a saturated chlorobenzene solution of phosphorus pentachloride (PCl_5) and illuminated at 100 °C for 1 h. The wafer was then put in a saturated diethyl ether solution of CH_3Li and kept for 2 h at room temperature. All the procedures were done under a dried argon atmosphere by use of the schlenk technique. The Si wafer thus methylated was finally washed with diethyl ether, ethanol and pure water.

The n-Si wafer was attached to a photoelectrochemical cell with an O-ring (effective area: 0.18 cm^2) in a form of a "window". Ohmic contact with n-Si was obtained with indium-gallium alloy. A platinum plate was used as the counter electrode, and an Ag|AgCl (sat. KCl) electrode was used as the reference electrode. Platinum nano-particles were deposited electrochemically on the methylated Si surface at −1.0 V vs. Ag|AgCl in 5 mM K_2PtCl_6 + 100 mM $LiClO_4$. The amount of electricity passing across the Si surface was 83 mC cm^{-2}. All chemicals were of reagent grade and used without further purification. Pure water with a resistivity of 18 MΩ cm^{-1} was obtained by a Milli-Q purification system.

Photocurrent density (j) vs. potential (U) was measured with a "Hokuto-Denko HSV-100 standard voltammetry tool", composed of a combination of potentiostat, potential programmer,

and recorder. The electricity passing across the electrode was measured with a digital coulomb meter (Nikko-Keisoku NDCM-3). Surface inspection was carried out with a Hitachi S-5000 high-resolution scanning electron microscope (SEM). X-ray photoelectron spectroscopic (XPS) analysis was performed with a Shimadzu ESCA-1000 spectrometer using an MgKα line.

Results and Discussion

The methylation of the n-Si surface by the above-described chemical treatment was confirmed by XPS analysis, as reported in Chapter 1. The methylated (CH_3-terminated) Si surface gave the carbon-1s XPS peak at 283.8 eV that was attributed to carbon in surface Si-CH_3 bonds, in contrast to non-methylated (H-terminated) Si surfaces. This assignment was in good agreement with the work reported by other researchers.[20,26] A very rough estimation of the surface coverage (θ) of CH_3 group from the C and Si XPS peaks, using the method of Himpsel et al.,[27] gave a value of around 70%, which was somewhat higher than a reported value of less than 50%[19] probably owing to an influence of contaminating organic compounds at the Si surface.

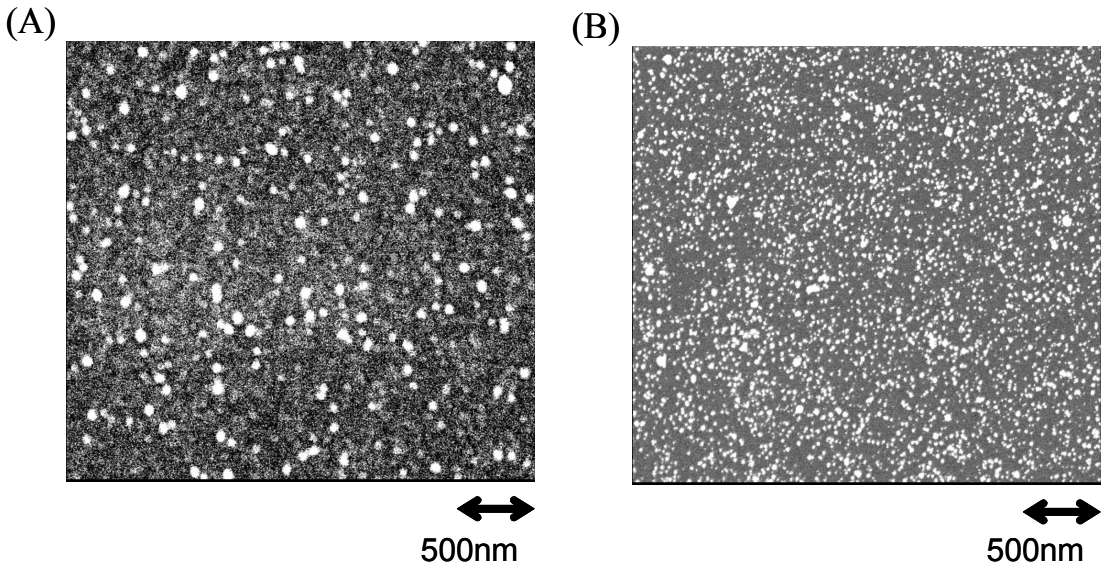

FIGURE 1 Scanning electron micrographs of (A) CH_3-terminated and Pt-dotted and (B) H-terminated and Pt-dotted n-Si surfaces just after Pt deposition.

Figure 1 shows scanning electron micrographs (SEM's) of (A) CH_3-terminated and Pt-dotted and (B) H-terminated and Pt-dotted n-Si surfaces just after Pt deposition. Circular Pt particles were deposited fairly homogeneously all over the n-Si surface in both cases, though

the size of the Pt particles for the CH_3-terminated and Pt-dotted n-Si was much larger, and the density of them was much less, than the corresponding values for the H-terminated and Pt-dotted n-Si. The current density vs. potential for electrodeposition of Pt on the CH_3-terminated n-Si was similar to that on the H-terminated n-Si, strongly suggesting that Pt for the CH_3-terminated n-Si was deposited on non-methylated (uncovered) parts of the Si surface, not on the methyl group of the methylated parts. It will be reasonable to assume that the methylated Si surface with the coverage of about 50% has non-methylated parts (domains) of nano-sizes here and there, at which Pt can be deposited.

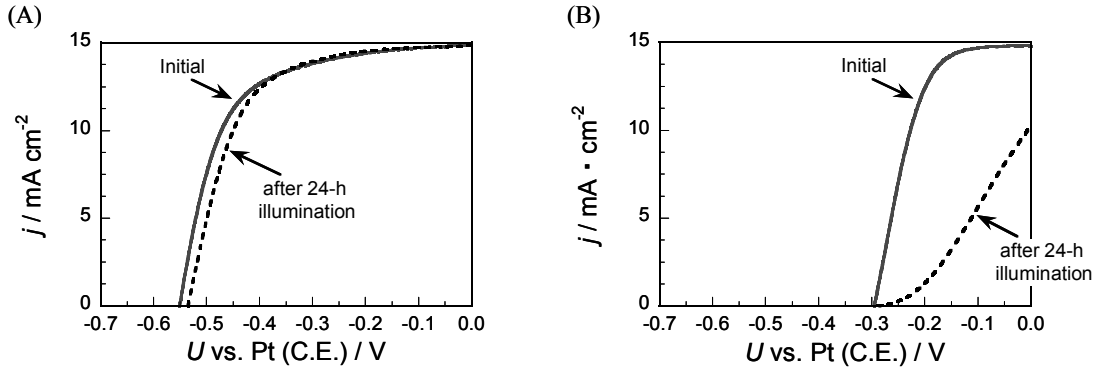

FIGURE 2 *j* vs. *U* curves for (A) CH_3-terminated and Pt-dotted and (B) H-terminated and Pt-dotted n-Si (111) electrodes in 7.6 M HI + 0.05 M I_2 under simulated solar (AM 1.5G, 100 mW cm^{-2}) illumination. Solid curves were observed at the initial stage, whereas dotted curves were observed after 24-h illumination.

Figure 2 shows the photocurrent density (*j*) vs. potential (*U*) for (A) CH_3-terminated and Pt-dotted and (B) H-terminated and Pt-dotted n-Si (111) electrodes in 7.6 M HI + 0.05 M I_2 under simulated solar (AM 1.5G, 100 mW cm^{-2}) illumination. Solid curves were observed at the initial stage, whereas dotted curves were observed after 24-h illumination. The CH_3-terminated and Pt-dotted n-Si electrode gave an efficient *j*-*U* curve, yielding a much

higher open-circuit photovoltage (V_{oc}) than the H-terminated and Pt-dotted n-Si electrode. It is to be emphasized that it is for the first time that such an efficient *j-U* curve as Figure 2(A) was obtained for n-Si in a redox electrolyte of 7.6 M HI + 0.05 M I_2 with a fairly less positive redox potential. This clearly indicates the effectiveness of Pt nano-contact and surface methylation. It is to be noted also that the *j-U* curve for the CH_3-terminated and Pt-dotted n-Si electrode was quite stable, showing almost no change during 24-h illumination, contrary to the case of the H-terminated and Pt-dotted n-Si electrode. This also indicates the effectiveness of the Pt nano-contact and surface methylation. Methylated but no Pt dotted n-Si electrodes showed only poor *j-U* curves, with the photocurrent starting at a fairly positive potential and increasing very gradually with the potential, though the *j-U* curves were stable for more than 30 min under continuous illumination, as already reported in Chapter 1.

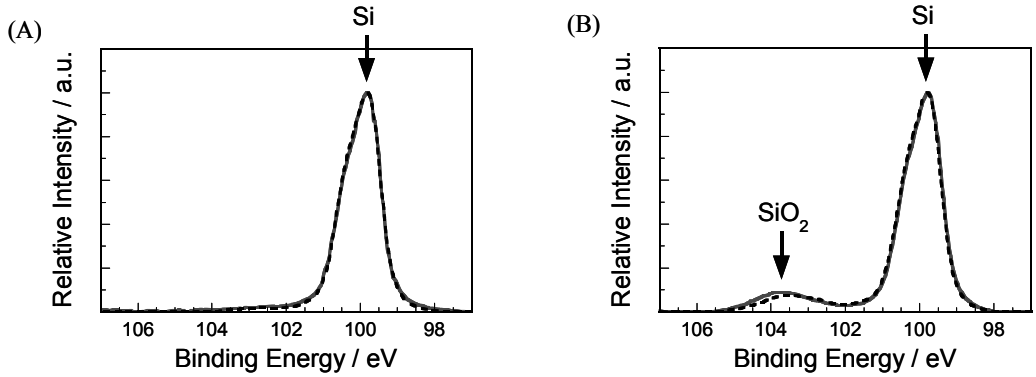

FIGURE 3 Si 2p XPS peaks for (A) CH_3-terminated and Pt-dotted and (B) H-terminated and Pt-dotted n-Si surfaces just after the Pt deposition. Solid curves were observed at the initial stage, whereas dotted curves were observed after 24-h illumination.

Figure 3 shows Si 2p XPS peaks for (A) CH_3-terminated and Pt-dotted and (B) H-terminated and Pt-dotted n-Si surfaces. Similarly to Figure 2, solid curves were observed at the initial stage just after the Pt deposition, whereas dotted curves were observed after the 24-h

illumination. The H-terminated and Pt-dotted n-Si showed an additional high-energy peak at 103.5 eV, attributed to formation of SiO_2 (Figure 3B), suggesting that the H-terminated n-Si(111) surface was slightly oxidized during the Pt deposition. The oxidation will occur at naked (non-Pt-deposited) parts of the Si surface, as reported.[7,8] The oxidation was prevented by the methylation (Figure 3A) most probably because the surface methyl group formed a hydrophobic thin layer on the Si surface and prevented the approach of water molecules to it. It is likely that the positive shift of the onset potential of the photocurrent (or a decrease in the V_{oc}) for the H-terminated and Pt-dotted n-Si electrode in Figure 2 is caused by the surface oxidation mentioned above, because the surface oxidation induces a positive shift in the flat-band potential (U_{fb}) of n-Si owing to the formation of an electrical double layer of surface dipoles ($Si^{\delta+}$–$O^{\delta-}$).

One may note that almost no further oxidation of the Si surface proceeded during the illumination in the (HI + I_2) solution for both the electrodes (Figures 3A and 3B), whereas the *j-U* curve for the H-terminated and Pt-dotted n-Si electrode degraded severely after the 24-h illumination (Figure 2B). The degradation can be attributed to gradual progress of the Si oxidation just beneath the Pt nano-particles, which leads to formation of a thin insulating layer between Si and Pt and thus the degradation in the *j-U* curve. An increase in the amount of the Si oxide by this oxidation may be negligible because only a very small part of the whole Si surface is covered with Pt nano-particles, thus resulting in almost no change in the XPS peak height.

A success of development of a new-type Si electrode with metal nano-contact and surface methylation has enabled us to accomplish efficient and stable solar to chemical conversion through photodecomposition of HI into H_2 and I_2 with no external bias. The key lies in that the photo-induced oxidation of I^- ions to iodine (I_2 or I_3^-) on this n-Si occurs at a potential more negative than hydrogen evolution on a Pt electrode, which implies that HI can

be decomposed into H_2 and I_2 (or I_3^-) with no external bias by such a cell as shown in Figure 4.

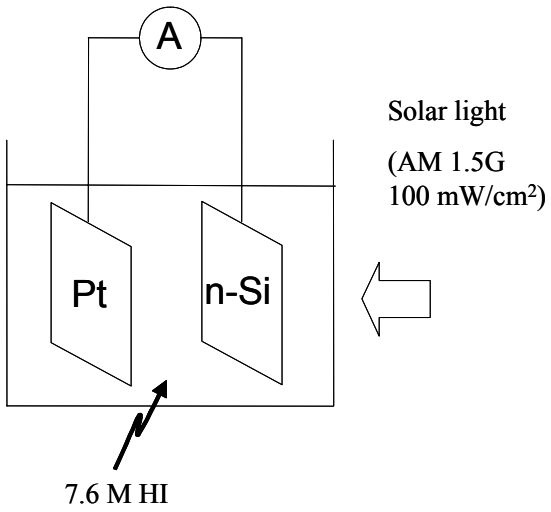

FIGURE 4 Schematic illustration of a photoelectrochemical cell for efficient solar decomposition of hydrogen iodide (HI) into hydrogen (H_2) and iodine (I_2 or I_3^-).

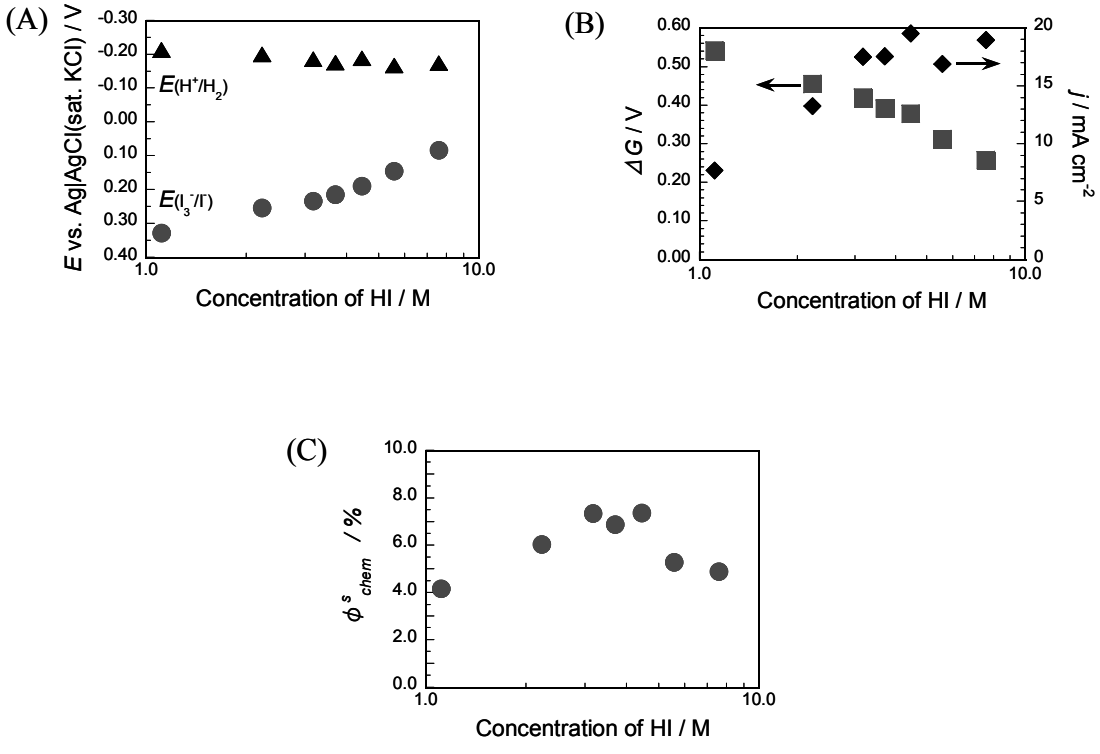

FIGURE 5 (A) The redox potentials for oxidation of I^- to I_2 (or I_3^-), $E(I_3^-/I^-)$, and hydrogen evolution, $E(H^+/H_2)$, (B) the Gibbs energy ΔG for the decomposition of HI into H_2 and I_2 (or I_3^-) and the observed photocurrent density (j), and (C) the solar to chemical conversion efficiency ϕ_{chem}^{s}, all plotted as a function of the concentration of HI.

The solar to chemical conversion efficiency ϕ_{chem}^{s} can be calculated by an equation

$$\phi_{chem}^{s} = \frac{(\Delta G / e) \times j}{\Delta E_s} \times 100(\%) \qquad (1)$$

where ΔG is the Gibbs energy (in a unit of eV) for the decomposition of HI into H_2 and I_2 (or I_3^-), e the elementary charge, j the observed photocurrent density (in a unit of mA cm^{-2}), and ΔE_s is the input solar energy (in a unit of mW cm^{-2}). Figure 5 shows the ΔG and j values, together with the redox potentials for the oxidation of I^- to I_2 (or I_3^-), $E(I_3^-/I^-)$, and hydrogen evolution, $E(H^+/H_2)$, measured as a function of the concentration of HI in the electrolyte. The $E(I_3^-/I^-)$ and $E(H^+/H_2)$ were determined from cyclic voltammograms with a Pt-plate electrode. Their dependences on the HI concentration should theoretically be given by the Nernst equation, though the activity coefficients in high HI concentrations will be deviated largely from unity and difficult to estimate. The Gibbs energy ΔG in Figure 5(B) was calculated from $E(I_3^-/I^-)$ and $E(H^+/H_2)$.

$$\Delta G/e = E(I_3^-/I^-) - E(H^+/H_2) \qquad (2)$$

The ϕ_{chem}^{s} in Figure 5(C) was calculated by equation (1). The author can see in Figure 5 that the ΔG decreases with the increasing HI concentration, whereas the j increases with it, and thus

the ϕ^{s}_{chem} takes a maximum at the HI concentration of 3.2 to 4.5 M. The maximum ϕ^{s}_{chem} value is 7.4 %, which is probably the highest of the solar to chemical conversion efficiencies ever reported, if he separate high values reported for molecular beam epitaxy (MBE)-prepared expensive high-quality composite multiplayer semiconductor electrodes such as p-n $Al_xGa_{1-x}As$/p-n Si[28] and p-n GaAs/p-$Ga_xIn_{1-x}P$/Pt.[29,30]

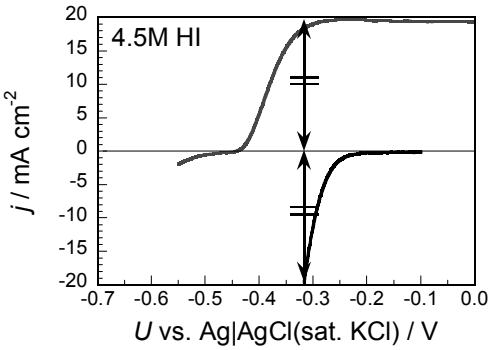

FIGURE 6 The *j*-*U* curves for the photo-oxidation of I^- on n-Si (111) and hydrogen evolution on Pt, in order to explain the principle of operation of the solar decomposition cell of Figure 4.

Figure 6 shows the *j*-*U* curve for the photo-induced oxidation of I^- ions to iodine (I_2 or I_3^-) on the CH_3-terminated and Pt-dotted n-Si (111) electrode, compared with that for the hydrogen evolution on a Pt plate electrode in the same electrolyte solution. The anodic current for the n-Si electrode and the cathodic current for a Pt electrode became equal in the absolute value at about −0.32 V, which explained the principle of operation of the solar decomposition cell of Figure 4. The conversion efficiency obtained in this chapter is high enough, as mentioned above, but this value can still be increased by optimization of the experimental parameters such as the coverage of the CH_3 group and the quantity and the size of the Pt particles. The matt-texture treatment of the n-Si surface to decrease the light reflectivity at the

surface will also be important in increasing the photocurrent density.

In conclusion, the author has revealed that an n-Si electrode with metal nano-contact and surface methylation gives a high V_{oc} even in a redox electrolyte of 7.6 M HI (or 7.6 M HI + 0.05 M I_2) and thus can be used for efficient solar to chemical conversion through photodecomposition of HI into H_2 and I_2. The solar to chemical conversion efficiency ϕ^{s}_{chem} reached a very high value of 7.4 % at the HI concentration of 3.2 to 4.5 M. It can be emphasized that it has long been believed that Si is unstable in aqueous electrolytes and useless for solar to chemical conversion, but the author has shown that the "unstable useless Si" can be converted to "stable useful Si". The combination of this method with low-cost Si materials such as amorphous Si or polycrystalline Si thin films will lead to realization of a high-efficiency and low-cost system for large-scale practical application of solar energy conversion.

References

(1) Center for Photovoltaic Engineering, UNSW (The University of New South Wales) Home Page. http://www.pv.unsw.edu.au/Research/scet.asp (accessed Jan 2006).

(2) Yamamoto, K.; Yoshimi, M.; Tawada, Y.; Fukuda, S.; Sawada, T.; Meguro, T.; Takata, H.; Suezaki, T.; Koi, Y.; Hayashi, K.; Suzuki, T.; Ichikawa, M.; Nakajima, A. *Sol. Energy Mater. Sol. Cells* **2002**, *74*, 449.

(3) Fujishima, A.; Honda, K. *Nature* **1972**, *238*, 37.

(4) Nozik, A. J.; Memming, R. *J. Phys. Chem.* **1996**, *100*, 13061.

(5) Nakato, Y. Photoelectrochemical Cells. In *Wiley Encyclopedia of Electrical and Electronics Engineering Online (www.interscience.wiley.com)*; Webster, J., Ed.; John Wiley & Sons, Inc., 2000.

(6) Nakato, Y.; Yano, H.; Tsubomura, H. *Chem. Lett.* **1986**, 987.

(7) Nakato, Y.; Ueda, K.; Yano, H.; Tsubomura, H. *J. Phys. Chem.* **1988**, *92*, 2316.

(8) Nakato, Y.; Tsubomura, H. *Electrochim. Acta* **1992**, *37*, 897.

(9) Yae, S.; Nakanishi, I.; Nakato, Y.; Toshima, N.; Mori, H. *J. Electrochem. Soc.* **1994**, *141*, 3077.

(10) Nakato, Y.; Kai, K.; Kawabe, K. *Sol. Energy Mater. Sol. Cells* **1995**, *37*, 323.

(11) Jia, J. G.; Fujitani, M.; Yae, S.; Nakato, Y. *Electrochim. Acta* **1997**, *42*, 431.

(12) Kawakami, K.; Fujii, T.; Yae, S.; Nakato, Y. *J. Phys. Chem. B* **1997**, *101*, 4508.

(13) Ishida, M.; Morisawa, K.; Hinogami, R.; Jia, J. G.; Yae, S.; Nakato, Y. *Z. Phys. Chem.* **1999**, *212*, 99.

(14) Linford, M. R.; Chidsey, C. E. D. *J. Am. Chem. Soc.* **1993**, *115*, 12631.

(15) Linford, M. R.; Fenter, P.; Eisenberger, P. M.; Chidsey, C. E. D. *J. Am. Chem. Soc.* **1995**, *117*, 3145.

(16) Bansal, A.; Li, X. L.; Lauermann, I.; Lewis, N. S.; Yi, S. I.; Weinberg, W. H. *J. Am. Chem. Soc.* **1996**, *118*, 7225.

(17) Sung, M. M.; Kluth, G. J.; Yauw, O. W.; Maboudian, R. *Langmuir* **1997**, *13*, 6164.

(18) Buriak, J. M. *Chem. Commun.* **1999**, 1051.

(19) Cicero, R. L.; Linford, M. R.; Chidsey, C. E. D. *Langmuir* **2000**, *16*, 5688.

(20) Okubo, T.; Tsuchiya, H.; Sadakata, M.; Yasuda, T.; Tanaka, K. *Appl. Surf. Sci.* **2001**, *171*, 252.

(21) Buriak, J. M. *Chem. Rev.* **2002**, *102*, 1271.

(22) Royea, W. J.; Juang, A.; Lewis, N. S. *Appl. Phys. Lett.* **2000**, *77*, 1988.

(23) Bansal, A.; Lewis, N. S. *J. Phys. Chem. B* **1998**, *102*, 4058.

(24) Cheng, J.; Robinson, D. B.; Cicero, R. L.; Eberspacher, T.; Barrelet, C. J.; Chidsey, C. E. D. *J. Phys. Chem. B* **2001**, *105*, 10900.

(25) Bansal, A.; Lewis, N. S. *J. Phys. Chem. B* **1998**, *102*, 1067.

(26) Terry, J.; Linford, M. R.; Wigren, C.; Cao, R. Y.; Pianetta, P.; Chidsey, C. E. D. *J. Appl. Phys.* **1999**, *85*, 213.

(27) Himpsel, F. J.; McFeely, F. R.; Talebibrahimi, A.; Yarmoff, J. A.; Hollinger, G. *Phys. Rev. B* **1988**, *38*, 6084.

(28) Licht, S.; Wang, B.; Soga, T.; Umeno, M. *Appl. Phys. Lett.* **1999**, *74*, 4055.

(29) Khaselev, O.; Turner, J. A. *Science* **1998**, *280*, 425.

(30) Khaselev, O.; Turner, J. A. *Electrochem. Solid State Lett.* **1999**, *2*, 310.

Chapter 3

Surface Structures, Photovoltages, and Stability of n-Si (111) Electrodes Surface-Modified with Metal Nano-Dots and Various Organic Groups

Abstract

The surface structures, photovoltages, and stability of n-Si(111) electrodes surface-modified with Pt nano-dots and organic groups were studied in an I_3^-/I^- redox electrolyte, using alkyls of varied chain length and those having a double bond and ester at the terminal as the organic groups. The n-Si was first modified with the organic groups and then Pt was electrodeposited on it. Linear sweep voltammetry revealed that for the modification with alkyls, the overvoltage for the Pt deposition became significantly larger with increasing the alkyl chain length, though this does not necessarily hold for the modification with alkyls having a double bond and ester. SEM inspection showed that the Pt-particle density decreased and the particle size increased, with increasing the alkyl chain length. The photovoltaic characteristics and stability for the n-Si electrodes modified with the organic groups were improved much by the Pt nano-dot coating, though they became somewhat inferior with increasing the alkyl chain length. Based on these results, it is concluded that the surface alkylation at high coverage together with the coating with small Pt nano-dots gives efficient and stable n-Si electrodes.

Introduction

Various approaches have been studied on photovoltaic solar energy conversion with the aim to realize high-efficiency and low-cost conversion systems for practical application on large scales. Of these, thin-film solar cells, such as amorphous Si solar cells, polycrystalline Si thin-film solar cells, and dye-sensitized TiO_2 solar cells, have been attracting much attention[1-3] because they are fabricated by use of inexpensive thin-film semiconductor materials. However, this approach has faced a serious deadlock in efficient current collection in large-area cells, because transparent conductive oxide (TCO) films, such as indium tin oxide (ITO), which are inevitably necessary in this approach, are expensive and moreover do not have a sufficiently high conductivity.

An alternative promising approach is direct solar to chemical conversion, such as solar water splitting, by use of a semiconductor/electrolyte junction.[4] The merits of this approach lie in that (1) inexpensive thin-film semiconductor materials can easily be utilized and (2) no current collection (and hence no TCO) is necessary. The latter is a great advantage in view of the above-mentioned difficulty of the thin-film solar cells. The main problem in this approach is that it is not easy to find efficient and stable semiconductor electrodes. For example, titanium dioxide (TiO_2) is stable and can photooxidize water into oxygen and H^+ ions,[5,6] but it only absorbs UV light. On the other hand, Si effectively absorbs solar light, but is unstable in aqueous electrolytes.

Recently, a number of studies have been made on modification of Si surfaces with organic alkyl groups with and without functional groups.[7-19] It is reported that the surface alkylation is effective to stabilize Si against surface oxidation.[20,21] However, it is also reported[22-27] that the attached surface alkyl groups retard interfacial electron transfer at the Si/redox electrolyte contacts. In Chapter 1, he reported that the dilemma could be solved by a combination of the surface alkylation with metal nano-dot coating, since the metal nano-dots

could act as an effective catalyst for interfacial electron transfer.[28-31] Moreover, a very high photovoltage could be generated for the electrodes of this type owing to a unique effect of metal nano-contact clarified in Chapter 2. With a Pt nano-dotted and methylated (CH_3-terminated) n-Si electrode, he succeeded in achieving efficient solar to chemical conversion through photodecomposition of hydrogen iodide (HI) into hydrogen (H_2) and iodine (I_2 or I_3^-). The efficiency reached 7.4% under simulated solar (AM 1.5G, 100 mW cm^{-2}) irradiation, which is, to his knowledge, the highest of the solar to chemical conversion efficiencies ever reported, apart from values obtained with expensive high-quality multilayer semiconductor electrodes.[32,33] The finding is important in that it opens a new possibility to convert Si that has long been regarded as unstable and useless in aqueous electrolytes to a stable and useful material.

In this chapter, he has made detailed studies on the modification of n-Si with various organic groups, including alkyls with varied chain lengths and those having the double bond and ester at the terminal, with an aim to find a way to get the further high performance and stability. The studies have shown that the size and the distribution of the metal nano-dots and the organic groups exert a strong influence on the photovoltaic characteristics and stability of the n-Si electrodes.

.

Experimental

Single crystal n-Si (111) wafers of the resistivity of 1 ~ 5 Ω cm and the thickness of 825±25 μm were donated by Osaka Tokushu-Gokin, Co. Ltd. The n-Si surface was cleaned by the RCA cleaning method [i.e. successive immersion in a boiling mixture of 95% H_2SO_4 and 30% H_2O_2 (3:1 in volume) for 15 min, 5% HF for 5 min, and a boiling mixture of 25% aqueous NH_3, 30% H_2O_2, and water (1:1:5 in volume) for 15 min]. The hydrogen (H)-terminated Si surface was obtained by immersion in 5% HF for 5 min, followed by immersion in 40% NH_4F for 15 min.

The modification of the n-Si surface with alkyls and those having the terminal C=C bonds was carried out by a method of photochlorination, followed by reaction with organolithium or organomagnesium, based on reports by Bansal et al.[9] and Okubo et al.[16] It is reported[19,34] that well ordered modified surfaces were obtained by this method. Experiments were done by illuminating an H-terminated n-Si (111) wafer in a saturated chlorobenzene solution of phosphorus pentachloride (PCl_5) with an ultrahigh pressure 500 W Hg lamp as the light source at 100°C for 1 h, to convert surface Si-H bonds to Si-Cl bonds. The wafer was then put in an organic solution of a carbanion reagent, such as 1.0 M methyl lithium (CH_3Li) in diethyl ether, 2.6 M *n*-butyl lithium (*n*-C_4H_9Li) or 1.9 M *n*-hexyl lithium (*n*-$C_6H_{13}Li$) in *n*-hexane, 1.0 M vinylmagnesium bromide (CH_2=CHMgBr) in THF, and 1.0 M 4-pentenyl lithium (CH_2=CH$(CH_2)_3Li$) in Et_2O/hexane, and refluxed for 3 h for CH_3Li, for 24 h for *n*-C_4H_9Li and *n*-$C_6H_{13}Li$, and for 48 h for CH_2=CHMgBr and CH_2=CH$(CH_2)_3Li$, to convert the Si-Cl bonds to Si-alkyl. All the procedures were carried out under a dried argon atmosphere by use of the schlenk technique. The surface-modified Si wafer thus obtained was finally washed with diethyl ether, 2-propanol, and pure water. The alkyl lithium and vinylmagnesium bromide used above were all commercially available, except that 4-pentenyl lithium was synthesized by the reaction of 5-bromo-1-pentene with lithium in Et_2O.

The modification with organic groups was also performed by a method of hydrosilylation of activated alkynes (HC≡CX, X=CO_2CH_3 and Ph).[35,36]

$$HC{\equiv}CX + {\equiv}Si\text{-}H_{\,s} \rightarrow {\equiv}Si\text{-}CH{=}CHX_{\,s} \qquad (1)$$

where the subscript "s" means the Si(111) surface. The reaction proceeded efficiently when freshly prepared H-terminated n-Si wafers were simply immersed in neat liquids of activated alkynes at room temperature for 24 to 40 h under irradiation of room light (from 40W fluorescent lamps lying about 2 m above the reaction vessel), with the reaction vessel being gently rotated. The efficient progress of the reaction was confirmed by X-ray photoelectron and IR spectroscopy, as explained in the next section. It is likely that, as the activated alkynes are very reactive, the reaction proceeds even under mild conditions, e.g., in the presence of a small amount of dissolved oxygen or under irradiation of room fluorescent light, by the same mechanisms as reported in the literature.[8,12-15,18] The detailed mechanism is now under investigation.

Pt nano-dots were deposited electrochemically. The n-Si wafer modified with the organic group was attached to an electrochemical cell in the form of a "window" with an O-ring (effective area: 0.18 cm^2). Ohmic contact with n-Si was obtained with indium-gallium alloy. The electrolyte was 5 mM K_2PtCl_6 + 100 mM $LiClO_4$. A platinum plate was used as the counter electrode, and an Ag|AgCl(sat. KCl) electrode was used as the reference electrode.

Linear sweep voltammetry (measurements of the Pt-deposition current under a negative potential sweep) and chronoamperometry (measurements of the Pt-deposition current at a fixed potential as a function of time) were performed with a commercial set of a potentiostat, a potential programmer, and a recorder (Hokuto-Denko HSV-100). The electricity passing across the electrode surface was measured with a digital coulomb meter (Nikko-Keisoku NDCM-3).

Photocurrent density (j) vs. potential (U), or solar cell characteristics for the n-Si electrodes were measured with the same electrochemical cell and apparatus as above, with the electrolyte being replaced by an aqueous I_3^-/I^- redox solution. A solar simulator (Kansai Kagaku Kikai XES-502S, AM 1.5 G, 100 mW cm^{-2}) was used as the light source. All chemicals were of reagent grade and used without further purification. Pure water of a resistivity of 18 MΩ cm^{-1} was obtained by a Milli-Q purification system.

Surface inspection was carried out with a Hitachi S-5000 high-resolution scanning electron microscope (SEM). X-ray photoelectron spectroscopic (XPS) analysis was performed with a Shimadzu ESCA-1000 spectrometer and a KRATOS-AXIS-165 spectrometer using an MgKα line.

Results

The methylation of the n-Si surface was confirmed by observation of the XPS C-1s peak at 283.8 eV, attributable to C in surface Si-CH_3 bonds,[37,38] as reported in Chapter 1. A rough estimation of the surface coverage (θ) for CH_3 from the C-1s and Si-2p peaks, using the method of Himpsel et al.,[39] gave a value of about 70 %, which was somewhat higher than a reported value of less than 50%[15] probably owing to an influence of C-1s peaks of contaminating hydrocarbons at the Si surface. The θ for alkyl groups with long chain lengths were difficult to determine because of decreased intensities of the 283.8-eV peak. The θ for organic esters were, on the other hand, obtained[35,36] with fluorinated alkynes, by measuring the relative intensities of the F-1s to Si-2p peaks at different take-off angles. By this way, the θ value for the modification with $HC{\equiv}CCO_2CH_2CF_3$ by immersion at room temperature under irradiation of room light (40W fluorescent lamps) for 24 h and 40 h was estimated to be 37 and 56%, respectively.

Figure 1 shows linear sweep voltammograms (LSV's) for the Pt electrodeposition on n-Si (111) modified with various organic groups, in 5 mM K_2PtCl_6 + 100 mM $LiClO_4$. The LSV's for H-terminated n-Si and one covered with a thin Si-oxide layer are included for reference. (The oxide layer was formed by immersion in a mixture of 95% H_2SO_4 and 30% H_2O_2 of 3:1 in volume for 15 min.) The potential was scanned from –0.05 V vs. Ag|AgCl toward the negative at a rate of 0.05 V s^{-1}. The Pt-deposition current for H-terminated n-Si started to increase (in the absolute value) at about –0.3 V, took a maximum at –0.72 V, and then decreased owing to diffusion limitation of $[PtCl_6]^{2-}$. The second increase in the current at about –1.0 V was due to hydrogen evolution. The LSV for methyl-terminated n-Si was similar in shape to that for H-terminated n-Si, but shifted in potential by about 0.05 V to the negative. The LSV's for n-Si modified with *n*-C_4H_9 and *n*-C_6H_{13} largely shifted to the negative, losing the current maximum. The negative shift became much more prominent with increasing the

alkyl chain length. On the other hand, the LSV's for n-Si modified with long alkyls having the terminal C=C bond and ester were rather similar to that for CH_3-terminated n-Si, with the clear current maximum.

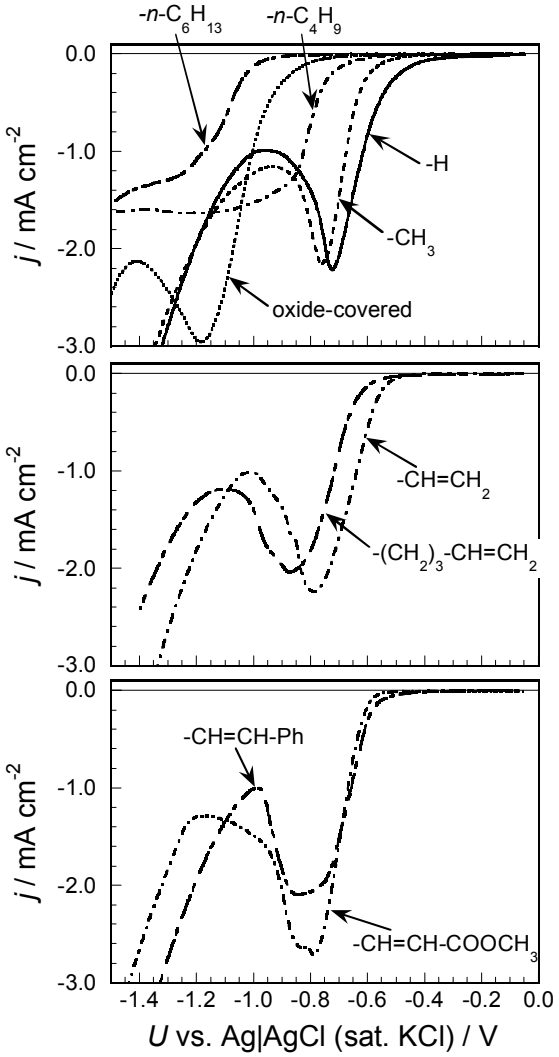

FIGURE 1 Linear sweep voltammograms for the Pt electrodeposition on n-Si(111) modified with various groups such as H, CH_3, *n*-C_4H_9, *n*-C_6H_{13}, -CH=CH_2, -$(CH_2)_3$-CH=CH_2, -CH=CH-Ph, and -CH=CH-$COOCH_3$. The curve marked by "oxide-covered" is for an n-Si electrode covered with a thin oxide layer. The electrolyte: 5 mM K_2PtCl_6 + 100 mM $LiClO_4$. The scan rate: 0.05 V s^{-1}.

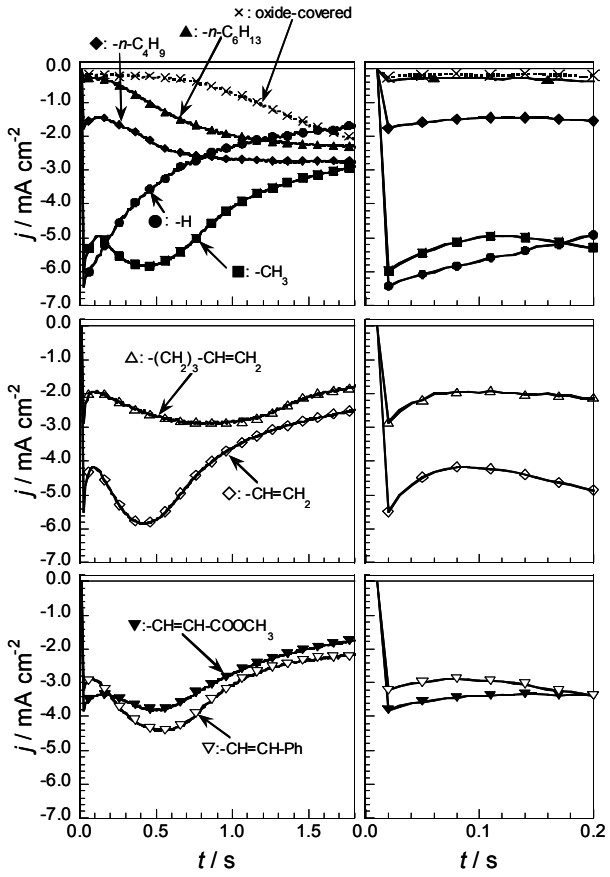

FIGURE 2 Chronoamperograms for the Pt electrodeposition on n-Si(111) modified with various groups such as H, CH_3, *n*-C_4H_9, *n*-C_6H_{13}, -CH=CH_2, -$(CH_2)_3$-CH=CH_2, -CH=CH-Ph, and -CH=CH-$COOCH_3$, together with that for "oxide-covered" n-Si. The potential was stepped from 0 to −1.0 V and kept at −1.0 V. The electrolyte: 5 mM K_2PtCl_6 + 100 mM $LiClO_4$. The figures on the right-hand side indicate sharp rise and decay of the current at the initial stage on an expanded time scale.

Figure 2 shows chronoamperograms for the Pt electrodeposition, obtained upon a potential step from 0 to −1.0 V, with the same electrodes and the same electrolyte as in Figure 1 being used. The Pt-deposition current for H-terminated n-Si showed an initial sharp rise, followed by a gradual decay exactly obeying the Cottrell equation,[40,41] indicating that the decay is due to the diffusion limitation of $[PtCl_6]^{2-}$. On the other hand, the current for n-Si modified

with CH_3, *n*-C_4H_9, and *n*-C_6H_{13} showed, in addition to the initial sharp rise and decay, the second gradual increase (and decay). Moreover, the initial sharp rise and decay became less prominent and the second gradual increase became more prominent, with increasing the alky chain length. The n-Si modified with alkyls having the terminal C=C bond and an organic ester showed similar behavior to those for alkyl-modified n-Si.

Figure 3 shows SEM images of the n-Si surfaces terminated with H, CH_3, *n*-C_4H_9, and *n*-C_6H_{13} just after the Pt deposition. The Pt deposition was carried out by the potential step from 0 to −1.0 V, as in Figure 2, followed by keeping the potential at −1.0 V until the fixed amount of electricity (83 mC cm^{-2}) passed across the electrode surface. For H-terminated n-Si, Pt was deposited homogeneously in the form of small nano-dots with the average diameter of about 6 nm. For CH_3-modified n-Si, a similar result was obtained, except that some of Pt dots grew to a large size of about 60 nm. For n-Si modified with long alkyls such as *n*-C_4H_9 and *n*-C_6H_{13}, most of Pt dots grew to large sizes. One may notice that the total amount of the deposited Pt is not the same among the electrodes of Figure 3, though the electricity passing across the Si surface was kept the same. This is mainly due to the fact that a part of the current contributes to hydrogen evolution, which occurs competitively with the Pt deposition, and the extent of its contribution strongly depends on the alkyl chain length. he can see from Figure 1 that the contribution of the hydrogen evolution to the current at −1.0 V (the Pt-deposition potential) decreases in the order, H- > CH_3- > C_4H_9- > C_6H_{13}-termination, and thus he can expect that the total amount of deposited Pt increases in this order. The prominent occurrence of hydrogen evolution for the H- and CH_3-terminated electrodes was also confirmed by observation of formation of gas bubbles at the Si surface after the Pt-deposition experiments.

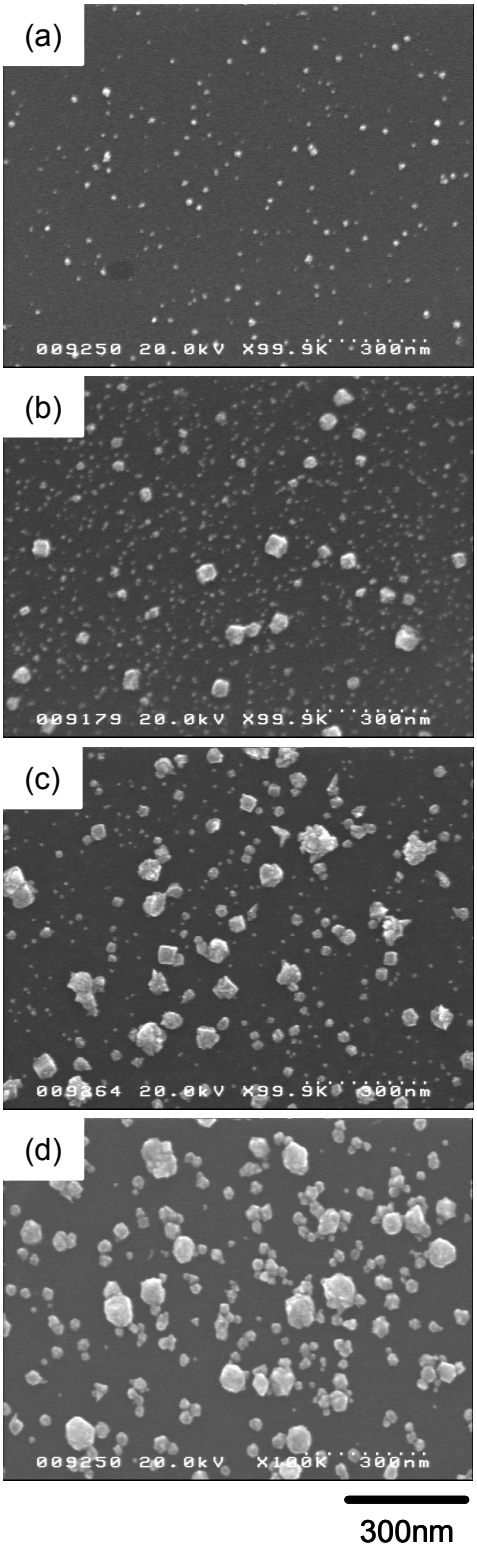

FIGURE 3 SEM images of the n-Si surfaces modified with (a) H, (b) CH_3, (c) n-C_4H_9, and (d) n-C_6H_{13} just after the Pt electrodeposition. The amount of electricity passing across the electrode surface was 83 mC cm^{-2} in all cases.

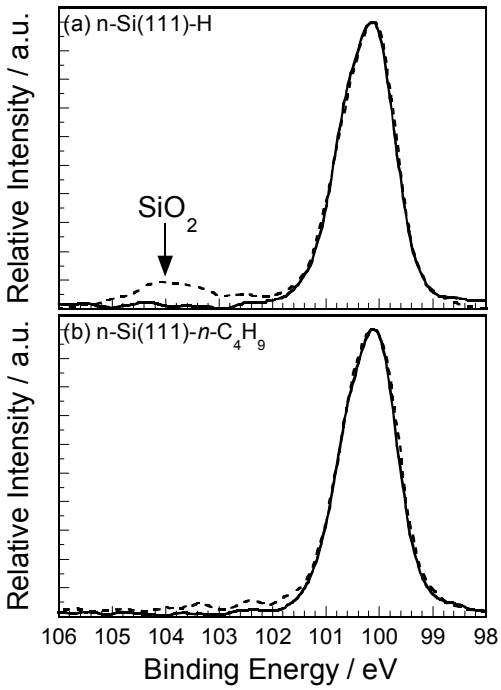

FIGURE 4 XPS Si-2p peaks for (a) H- and (b) *n*-C_4H_9-modified n-Si, (solid curve) before and (dashed curve) after the Pt electrodeposition.

Figure 4 shows, as typical examples, XPS Si-2p peaks for (a) H-terminated and (b) *n*-C_4H_9 modified n-Si before and after the Pt deposition. The H-terminated n-Si after the Pt deposition showed a clear peak at 104 eV, attributable to formation of SiO_2, contrary to n-Si before the Pt deposition. The effective surface oxidation in Pt-dotted (naked) n-Si in aqueous solutions is reported[42] by Yae et al. and explained to be due to hole injection into the valence band by dissolved oxygen via deposited Pt as a catalyst. On the other hand, the *n*-C_4H_9 modified n-Si showed almost no (or only a weak) peak at 104 eV even after the Pt deposition. The n-Si modified with CH_3 (in Chapter 2) and *n*-C_6H_{13} gave similar results to Figure 4(b), indicating that the organic modification effectively prevented the oxidation of the Si surface.

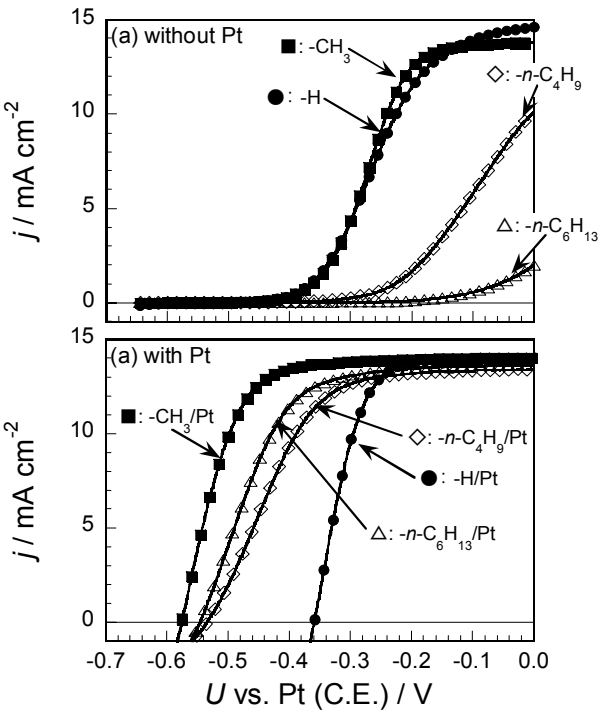

FIGURE 5 *j* - *U* characteristics for n-Si (111) modified with (●) H, (■) CH_3, (◇) *n*-C_4H_9, and (△) *n*-C_6H_{13}, without and with Pt nano-dots, under simulated solar (AM 1.5G, 100 mW cm^{-2}) illumination. The electrolyte was 7.6 M HI + 0.05 M I_2. The scan rate was 0.05 V s^{-1}.

Figure 5 compares photocurrent (*j*) vs. potential (*U*) characteristics in 7.6 M HI + 0.05 M I_2 for various alkyl modified n-Si (111) with and without Pt. For no Pt nano-dot coating (Figure 5a), the CH_3-modified n-Si showed a similar characteristic to the H-terminated one, whereas the *n*-C_4H_9- and *n*-C_6H_{13}-modified n-Si showed much less efficient characteristics, only with gradually increasing low *j*. The Pt deposition improved the characteristics for the alkyl modified n-Si very much (Figure 5b), though they slightly depended on the alkyl chain length. Table 1 summarizes solar-cell parameters such as the open-circuit photovoltage V_{oc}, the short circuit photocurrent j_{sc}, the fill factor *F.F.*, and the solar energy conversion efficiency η,

for various n-Si electrodes. The η values in Table 1 are lower than those reported previously by the group he belongs to,[28-31] which is mainly due to the low j_{sc} caused by a particular cell structure with a long optical path in the colored electrolyte in the present work.

TABLE 1 Solar cell characteristics for n-Si (111) modified with various alkyls, with and without Pt nano-dots. Those for the H-terminated and oxide-covered n-Si are also included for reference. V_{oc}: the open-circuit photovoltage, j_{sc}: the short-circuit photocurrent density, *F.F.*: the fill factor, η: the solar energy conversion efficiency.

Surface alkyl	without Pt				with Pt nano-dots			
	V_{oc} / V	j_{sc} / mAcm^{-2}	*F.F.*	η / %	V_{oc} / V	j_{sc} / mAcm^{-2}	*F.F.*	η / %
H	0.502	14.59	0.312	2.29	0.359	13.95	0.653	3.27
CH_3	0.515	13.77	0.357	2.53	0.576	14.03	0.702	5.67
n-C_4H_9	0.466	10.12	0.124	0.58	0.535	13.41	0.568	4.07
n-C_6H_{13}	0.442	1.99	0.177	0.16	0.546	13.63	0.616	4.59

Figure 6 shows results of stability tests for various alkyl modified n-Si with Pt nano-dots in 7.6 M HI + 0.05 M I_2, in which the *j*-*U* curves at the initial stage and after 24-h continuous illumination are compared. Figure 7 shows time courses of the η value (which is in proportion to the $|j \times U|$ at the maximum power point), calculated from the same results as in Figure 6. The sudden increase in the η value for the CH_3-modified n-Si at the 24-h illumination indicates that the η was recovered by replacement of the old electrolyte with a fresh one. This result implies that the η decay for this electrode in Figure 7 (except the initial one) is only due to coloring of the electrolyte by an increase in the I_2 (or I_3^-) concentration through air oxidation during illumination. This argument is supported by the fact that even after the 24-h illumination, the CH_3-modified n-Si showed no growth of the surface oxide, as estimated from the XPS Si-2p peaks. On the other hand, the n-Si modified with long-chain alkyls such as

n-C_6H_{13} showed gradual degradation of the solar cell characteristics (Figures 6 and 7). SEM inspection showed that a considerable part of Pt dots of large sizes were peeled off from the Si surface after the long-term illumination.

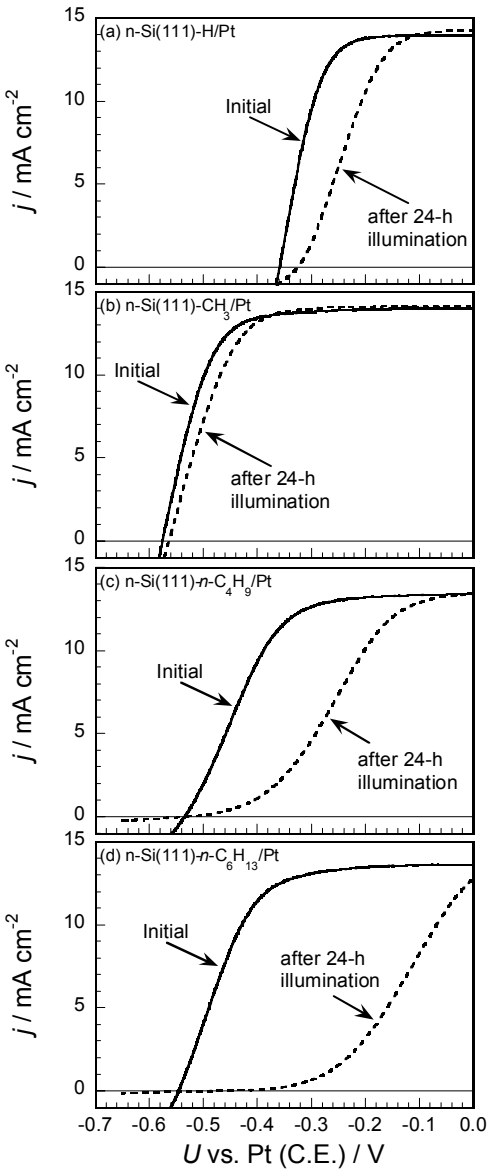

FIGURE 6 The *j* - *U* characteristics for n-Si modified with (a) H, (b) CH_3, (c) *n*-C_4H_9, and (d) *n*-C_6H_{13}, all with Pt nano-dots, (solid curve) at the initial stage and (dashed curve) after continuous 24-h illumination. The light source: a solar simulator (AM 1.5G, 100 mW cm^{-2}). The electrolyte: 7.6 M HI + 0.05 M I_2. The scan rate: 0.05 V s^{-1}.

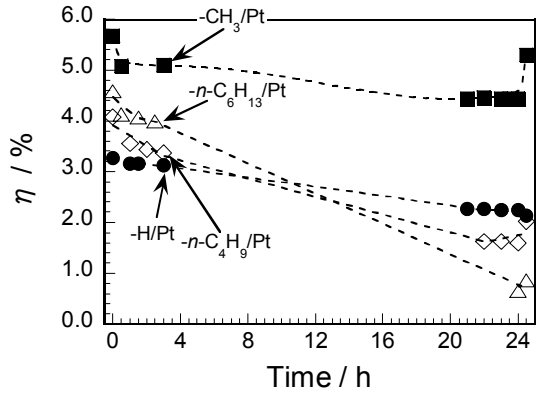

FIGURE 7 Time courses of the solar energy conversion efficiency (η) for n-Si modified with (●) H, (■) CH_3, (◇) n-C_4H_9, and (△) n-C_6H_{13}, all with Pt nano-dots, under continuous simulated-solar (AM 1.5G, 100 mW cm^{-2}) illumination. The electrolyte solution was 7.6 M HI + 0.05 M I_2. The sudden increase in η for CH_3-modified n-Si at the 24-h illumination is due to replacement of the old electrolyte with a fresh one.

Discussion

The experimental results show that the photovoltaic characteristics and stability for the surface alkylated and Pt nano-dotted n-Si electrodes strongly depend on how the alkyl groups and Pt nano-dots are attached and distributed on the Si surface. Let him first consider the Pt-electrodeposition process at the alkyl-modified n-Si surfaces. Little work has, to his knowledge, been done on this process, in contrast to the metal electrodeposition on H-terminated n-Si surfaces.[43-45] Figure 8 illustrates a plausible model for the Pt electrodeposition on the alkyl modified n-Si surface. Here it is convenient to define two kinds of the surface coverage for organic groups: $\theta_{Si\text{-}C}$ and θ_{hole}, where the $\theta_{Si\text{-}C}$ refers to the ratio of the density of Si-C bonds ($N_{Si\text{-}C}$) against the density of the outermost Si atoms (N_{Si}) at the Si (111) surface ($\theta_{Si\text{-}C} = N_{Si\text{-}C}/N_{Si}$), whereas the θ_{hole} refers to the ratio of the density of holes (uncovered domains) (N_{hole}) in the attached organic layer against the N_{Si} ($\theta_{hole} = N_{hole}/N_{Si}$).

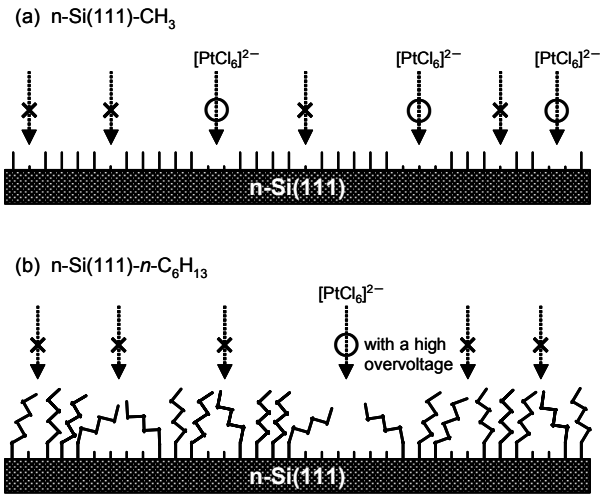

FIGURE 8 Schematic illustrations of the Pt electrodeposition process on the (a) CH_3- and (b) n-C_6H_{13}-modified n-Si (111) surface. Vertical short lines at the Si surface refer to non-alkylated Si sites, vertical long lines refer to CH_3-attached sites, and zigzag lines indicate n-C_6H_{13}. Arrows with open circles mean that the Pt deposition can occur, whereas arrows with cross marks indicate that it cannot occur.

The main features of Figure 8 are summarized as follows: (1) The surface modification with organic groups does not proceed completely and thus the $\theta_{Si\text{-}C}$ is less than unity (the $\theta_{Si\text{-}C}$ is about 40 to 70 %, as estimated from the XPS data). (2) For short-alkyl (CH_3)-modified n-Si, the θ_{hole} is expected to be nearly equal to the $\theta_{Si\text{-}C}$, whereas for long-alkyl modified n-Si, the θ_{hole} is much less than the $\theta_{Si\text{-}C}$. In other words, the θ_{hole} becomes lower as the alkyl-chain length gets longer. This feature comes from a consideration that long alkyl chains attached to the surface lie down on adjacent non-alkylated Si sites and cover these sites, as schematically shown in the lower part of Figure 8. (3) The Pt deposition will occur only at the hole parts (uncovered parts) in the attached organic layer and thus the θ_{hole} determines the density of the deposited Pt particles. This feature comes from the following considerations. The Pt electrodeposition on Si from an aqueous $[PtCl_6]^{2-}$ solution is expected to occur via adsorption of $[PtCl_4]^{2-}$ ions, similarly to the case of electrodeposition of Pd on Au (111) reported.[46,47] This implies that the Pt deposition should occur at non-alkylated Si sites at which the adsorption energy is the largest. More strictly, as the anionic reactant, $[PtCl_4]^{2-}$, has a large hydration sphere, the Pt deposition might occur only at a part of assemblies of non-alkylated Si sites with appropriately wide areas, as shown in the upper part of Figure 8, though further studies are needed to get a definite conclusion on this point.

Now, on the basis of the above model, the SEM images of Figure 3 can be explained as follows. For H-terminated n-Si, the Pt deposition can occur at any place of the Si surface, thus leading to formation of a high density of crystalline nuclea for Pt growth and hence a high density of Pt nano-dots. For alkyl-modified n-Si, the Pt nuclea will be formed only at the holes in the attached organic layer, as mentioned above. However, for short-alkyl (CH_3)-modified n-Si, the θ_{hole} is still high, and thus a moderately high density of Pt nano-dots is formed. For n-Si modified with long alkyls such as n-C_4H_9 and n-C_6H_{13}, the θ_{hole} becomes low, and thus only a low density of Pt nano-dots is formed. The size of the Pt nano-dots becomes larger with

the decreasing Pt density, because the total electricity passing across the Si surface is kept constant (83 mC cm^{-2}). The total amount of the deposited Pt does not look the same among the surfaces of Figure 3. This can be attributed to the difference in the contribution of hydrogen evolution, which competitively occurs with the Pt deposition, as already mentioned in the preceding section.

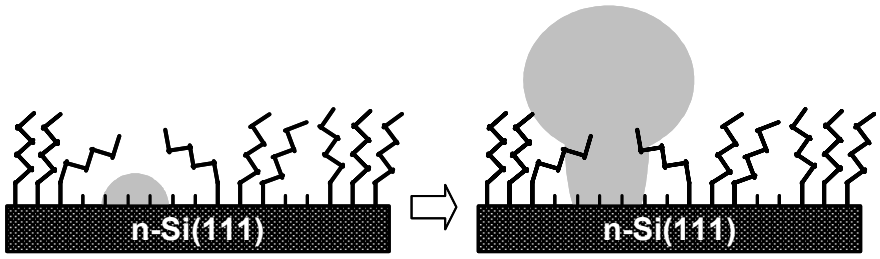

FIGURE 9 Schematic illustration of two-step Pt growth on the alkyl-modified n-Si (111) surface.

The above model can explain the chronoamperograms in Figure 2 as well. For H-terminated n-Si, the Pt deposition proceeds with a high density of Pt nuclea, thus producing a nearly linear diffusion layer on the n-Si surface. This implies that the deposition-current shows an initial sharp rise, followed by a gradual decay obeying the Cottrell equation, as really observed. For alkylated n-Si, the peak height for the initial sharp-rising current decreases with increasing the alkyl chain length (Figure 2). This can be attributed partly to a decrease in the θ_{hole} and partly to an increase in the activation energy for the Pt deposition discussed later. For the alkylated n-Si, the deposition current shows the second gradual increase and decay (Figure 2). This can be attributed to successive Pt deposition on the initially formed Pt nano-dots (Figure 9). The key is that if the initially formed Pt nano-dots are sparsely distributed, the successive Pt deposition produces a spherical diffusion layer around the Pt nano-dots, which leads to the increase in the deposition current. This explanation is in agreement with the

formation of the large Pt nano-dots for the alkylated n-Si (Figure 3). Moreover, this explanation is supported by reported work,[48,49] in which the similar gradual current increase and decay for metal electrodeposition were explained quantitatively by a 3D crystallite nucleation and growth mechanism, in the same way as in the present work.

How can he explain the dependence of the LSV's on the alkyl chain length (the uppermost figure of Figure 1)? The negative potential shifts in the LSV's for the alkylated n-Si compared with the H-terminated one are most probably due to the increases in the overvoltage (or the activation energy) for the Pt deposition by the alkyl modification. The increases in the overvoltage will arise partly from steric hindrance of alkyl chains to $[PtCl_6]^{2-}$ diffusion from the solution bulk to the Si surface and partly from a decrease in the adsorption energy of the anionic reactant ($[PtCl_4]^{2-}$) by surrounding alkyl groups. These factors will become more important with increasing the alkyl chain length. Here he has to note that the negative potential shifts in the LSV's (or the overvoltages for the Pt deposition) for the modification with alkyls having functional groups such as C=C and ester are much smaller than those for the modification with simple alkyls with similar chain lengths (middle and lower figures of Figure 1). The detailed mechanism for this result is unknown at present. A tentative explanation might be given by assuming either a slight hydrophilic nature of the functional groups or a morphologically flexible nature of alkyl chains containing C=C or C-O-C bonds.

In relation to the above argument, it is interesting to note a recent paper[50] reporting that the alkyl modification of the Si surface causes a negative shift of about 0.4 V in the flat-band potential (U_{fb}). The concept of the shift in the U_{fb} by the surface modification[50,51] may provide another possibility to explain the negative potential shifts in the LSV's. However, the shift in the LSV's between the H- and CH_3-modification in Figure 1 is only 0.05 V and that between the CH_3- and C_4H_9-modification is about 0.12 V, which are both much smaller than the reported 0.4 V. Besides, the solar cell characteristics for alkylated n-Si electrodes, explained

below, are not necessarily in harmony with the assumption of the shifts in the U_{fb}. Anyhow, further studies are necessary to clarify the above problem.

Next, let him consider the solar cell characteristics for the Pt nano-dotted and surface alkylated n-Si electrodes. It is reported[22-27] that the surface alkylation tends to retard interfacial electron transfer at the semiconductor/redox electrolyte interface. In fact, the surface alkylated n-Si electrodes with no Pt dots show less efficient characteristics (Figure 5). The drastic improvement in the characteristics (in particular, the open-circuit photovoltage, V_{oc}) by the Pt deposition (Figure 5) thus clearly indicates that the Pt nano-dots deposited at non-alkylated Si sites (Figures 8 and 9) act as an efficient catalyst for electrode reactions (or an effective gate for interfacial hole transport). If Pt were deposited on the alkyl group attached to the Si surface, it could not act as the effective gate, because the intervening insulating alkyl group gives rise to a large electric resistance. The result of Figure 5 thus gives strong support to the model of the direct Pt-Si contact, such as shown in Figures 8 and 9.

Comparison of the solar-cell characteristics for n-Si modified with various alkyl groups and Pt nano-dots indicates that the CH_3-modified n-Si gives the best characteristic (Figure 5 and Table 1). The slightly decreased V_{oc} for n-Si modified with n-C_4H_9 and n-C_6H_{13} can be attributed to the increase in the area of direct Pt-Si contact, caused by the increase in the size of the Pt nano-dots (Figure 3). The group he belongs to discussed in detail previously[28-31] that the increase in the area of direct Pt-Si contact causes the decrease in the effective barrier height and hence the decrease in the V_{oc}. The decreased fill factor (*F.F.*) for the n-Si modified with n-C_4H_9 and n-C_6H_{13} (Figure 3 and Table 1) may be attributed to low densities of the Pt nano-dots (Figure 3), which leads to a high current density in the area of the direct Pt-Si contact as well as at the Pt/electrolyte interface and hence large ohmic losses.

Finally, let him consider the electrode stability. The η value (or the maximum power) for the CH_3-modified n-Si shows no decay during the continuous 24-h illumination, except the

initial small drop (Figure 7), indicating that this electrode has a high stability. In harmony with the result, the CH_3-modified n-Si showed no growth of the surface oxide during the 24-h illumination. On the other hand, the η value for the n-Si modified with long-chain alkyls such as *n*-C_4H_9 and *n*-C_6H_{13} shows gradual decays (Figure 7) mainly owing to decreases in the *F.F.* (Figure 6). The decreased stability for the long-chain alkyl modified n-Si can be attributed to a mechanical loss (peeling off) of the deposited Pt dots of large sizes during the long-term experiments with electrolyte stirring, as indicated by the SEM inspection.

In conclusion, the present work has revealed that the alkyl chain length and the functional group of modifying organic groups strongly affect the modifying reaction as well as the Pt-electrodeposition process, which in turn exerts a strong influence on the solar cell characteristics and stability of the electrodes. The detailed analyses have indicated that the coating with small Pt nano-dots is effective for obtaining highly efficient solar cell characteristics and that the high coverage of the organic group as well as small Pt nano-dots is crucial for high stability. The experimental results have also shown that the CH_3-modified and Pt nano-dotted n-Si nearly meets these conditions, thus yielding efficient and stable characteristics. The present result is of high importance, in that it has given a definite way to obtain efficient and stable n-Si electrodes for solar to chemical conversion.

References

(1) Chopra, K. L.; Paulson, P. D.; Dutta, V. *Prog. Photovolt.* **2004**, *12*, 69.

(2) Goetzberger, A.; Hebling, C.; Schock, H. W. *Mater. Sci. Eng., R* **2003**, *40*, 1.

(3) Shah, A.; Torres, P.; Tscharner, R.; Wyrsch, N.; Keppner, H. *Science* **1999**, *285*, 692.

(4) Tryk, D. A.; Fujishima, A.; Honda, K. *Electrochim. Acta* **2000**, *45*, 2363.

(5) Fujishima, A.; Kohayakawa, K.; Honda, K. *Bull. Chem. Soc. Jpn.* **1975**, *48*, 1041.

(6) Fujishima, A.; Kohayakawa, K.; Honda, K. *J. Electrochem. Soc.* **1975**, *122*, 1487.

(7) Linford, M. R.; Chidsey, C. E. D. *J. Am. Chem. Soc.* **1993**, *115*, 12631.

(8) Linford, M. R.; Fenter, P.; Eisenberger, P. M.; Chidsey, C. E. D. *J. Am. Chem. Soc.* **1995**, *117*, 3145.

(9) Bansal, A.; Li, X. L.; Lauermann, I.; Lewis, N. S.; Yi, S. I.; Weinberg, W. H. *J. Am. Chem. Soc.* **1996**, *118*, 7225.

(10) Sieval, A. B.; Demirel, A. L.; Nissink, J. W. M.; Linford, M. R.; van der Maas, J. H.; de Jeu, W. H.; Zuilhof, H.; Sudholter, E. J. R. *Langmuir* **1998**, *14*, 1759.

(11) Allongue, P.; de Villeneuve, C. H.; Pinson, J.; Ozanam, F.; Chazalviel, J. N.; Wallart, X. *Electrochim. Acta* **1998**, *43*, 2791.

(12) Buriak, J. M. *Chem. Commun.* **1999**, 1051.

(13) Strother, T.; Cai, W.; Zhao, X. S.; Hamers, R. J.; Smith, L. M. *J. Am. Chem. Soc.* **2000**, *122*, 1205.

(14) Sieval, A. B.; Linke, R.; Zuilhof, H.; Sudholter, E. J. R. *Adv. Mater.* **2000**, *12*, 1457.

(15) Cicero, R. L.; Linford, M. R.; Chidsey, C. E. D. *Langmuir* **2000**, *16*, 5688.

(16) Okubo, T.; Tsuchiya, H.; Sadakata, M.; Yasuda, T.; Tanaka, K. *Appl. Surf. Sci.* **2001**, *171*, 252.

(17) Wayner, D. D. M.; Wolkow, R. A. *J. Chem. Soc., Perkin Trans. 2* **2002**, 23.

(18) Buriak, J. M. *Chem. Rev.* **2002**, *102*, 1271.

(19) Yu, H. B.; Webb, L. J.; Ries, R. S.; Solares, S. D.; Goddard, W. A.; Heath, J. R.; Lewis, N. S. *J.*

Phys. Chem. B **2005**, *109*, 671.

(20) Bansal, A.; Lewis, N. S. *J. Phys. Chem. B* **1998**, *102*, 4058.

(21) Royea, W. J.; Juang, A.; Lewis, N. S. *Appl. Phys. Lett.* **2000**, *77*, 1988.

(22) Bansal, A.; Lewis, N. S. *J. Phys. Chem. B* **1998**, *102*, 1067.

(23) Yu, H. Z.; Boukherroub, R.; Morin, S.; Wayner, D. D. M. *Electrochem. Commun.* **2000**, *2*, 562.

(24) Barrelet, C. J.; Robinson, D. B.; Cheng, J.; Hunt, T. P.; Quate, C. F.; Chidsey, C. E. D. *Langmuir* **2001**, *17*, 3460.

(25) Cheng, J.; Robinson, D. B.; Cicero, R. L.; Eberspacher, T.; Barrelet, C. J.; Chidsey, C. E. D. *J. Phys. Chem. B* **2001**, *105*, 10900.

(26) Zhao, J. W.; Uosaki, K. *Appl. Phys. Lett.* **2003**, *83*, 2034.

(27) Niwa, D.; Inoue, T.; Fukunaga, H.; Akasaka, T.; Yamada, T.; Homma, T.; Osaka, T. *Chem. Lett.* **2004**, *33*, 284.

(28) Nakato, Y.; Ueda, K.; Yano, H.; Tsubomura, H. *J. Phys. Chem.* **1988**, *92*, 2316.

(29) Nakato, Y.; Tsubomura, H. *Electrochim. Acta* **1992**, *37*, 897.

(30) Jia, J. G.; Fujitani, M.; Yae, S.; Nakato, Y. *Electrochim. Acta* **1997**, *42*, 431.

(31) Ishida, M.; Morisawa, K.; Hinogami, R.; Jia, J. G.; Yae, S.; Nakato, Y. *Z. Phys. Chem.* **1999**, *212*, 99.

(32) Khaselev, O.; Turner, J. A. *Science* **1998**, *280*, 425.

(33) Licht, S.; Wang, B.; Soga, T.; Umeno, M. *Appl. Phys. Lett.* **1999**, *74*, 4055.

(34) Webb, L. J.; Lewis, N. S. *J. Phys. Chem. B* **2003**, *107*, 5404.

(35) Liu, Y.; Yamazaki, S.; Yamabe, S. *J. Org. Chem.* **2005**, *70*, 556.

(36) Liu, Y.; Yamazaki, S.; Yamabe, S.; Nakato, Y. *J. Mater. Chem.* **2005**, *15*, 4906.

(37) Liu, H. B.; Hamers, R. J. *Surf. Sci.* **1998**, *416*, 354.

(38) Terry, J.; Linford, M. R.; Wigren, C.; Cao, R. Y.; Pianetta, P.; Chidsey, C. E. D. *J. Appl. Phys.* **1999**, *85*, 213.

(39) Himpsel, F. J.; McFeely, F. R.; Talebibrahimi, A.; Yarmoff, J. A.; Hollinger, G. *Phys. Rev. B* **1988**, *38*, 6084.

(40) Cottrell, F. G. *Z. Physik. Chem.* **1902**, *42*, 385.

(41) Bard, A. J.; Faulkner, L. R. *Electrochemical Methods: Fundamentals and Applications*, 2nd. ed.; John Wiley & Sons: New York, 2001; pp 156 ff.

(42) Yae, S.; Kawamoto, Y.; Tanaka, H.; Fukumuro, N.; Matsuda, H. *Electrochem. Commun.* **2003**, *5*, 632.

(43) Yae, S.; Kitagaki, M.; Hagihara, T.; Miyoshi, Y.; Matsuda, H.; Parkinson, B. A.; Nakato, Y. *Electrochim. Acta* **2001**, *47*, 345.

(44) Munford, M. L.; Maroun, F.; Cortes, R.; Allongue, P.; Pasa, A. A. *Surf. Sci.* **2003**, *537*, 95.

(45) dos Santos, M. C.; Geshev, J.; Pereira, L. G.; Alves, M. C. M.; Schmidt, J. E.; Allongue, P. *Phys. Rev. B* **2004**, *70*, 104420.

(46) Naohara, H.; Ye, S.; Uosaki, K. *J. Phys. Chem. B* **1998**, *102*, 4366.

(47) Naohara, H.; Ye, S.; Uosaki, K. *J. Electroanal. Chem.* **1999**, *473*, 2.

(48) Oskam, G.; Long, J. G.; Natarajan, A.; Searson, P. C. *J. Phys. D: Appl. Phys.* **1998**, *31*, 1927.

(49) Hyde, M. E.; Compton, R. G. *J. Electroanal. Chem.* **2003**, *549*, 1.

(50) Lie, L. H.; Patole, S. N.; Hart, E. R.; Houlton, A.; Horrocks, B. R. *J. Phys. Chem. B* **2002**, *106*, 113.

(51) Cohen, R.; Zenou, N.; Cahen, D.; Yitzchaik, S. *Chem. Phys. Lett.* **1997**, *279*, 270.

Chapter 4

Negative Shifts in the Flat-band Potential by Adsorption of Iodide Ions on Surface-alkylated and Pt Nano-dotted n-Si(111) Electrodes for Improvement of Solar Cell Characteristics

Abstract

The flat-band potential (U_{fb}) and solar cell characteristics for surface-alkylated and Pt nano-dotted n-Si (111) electrodes have been studied in I_3^-/I^- redox electrolytes, using various alkyls as the surface terminating group. It is found that the U_{fb} for the surface-methylated and Pt nano-dotted n-Si (111) electrodes shifts toward the negative with increasing the I^- concentration in the electrolyte, in parallel to the equilibrium redox potential $U_{eq}(I_3^-/I^-)$, and thus the open-circuit photovoltage V_{oc} remains nearly constant among various I_3^-/I^- redox electrolytes with different $U_{eq}(I_3^-/I^-)$. The constant V_{oc} is observed only for the I_3^-/I^- redox couples with varied I^- concentrations and not for other redox couples, indicating that it is not caused by the Fermi level pinning via a surface state. The U_{fb} shift with the I^- concentration is explained in terms of the I^- adsorption in the form of a Si-I···I^- complex at surface Si-I bonds, which are formed at non-modified (naked) Si sites. The n-Si electrodes modified with long-chain alkyls show similar negative shifts in the U_{fb} by the iodine adsorption. The U_{fb} measurements in the dark and under illumination have also shown that the Pt nano-dots act as an efficient catalyst (gate) for interfacial electron transfer.

Introduction

Silicon (Si) is the most suitable semiconductor for solar energy conversion[1,2] in view of an appropriate band-gap of 1.1 eV for obtaining a high efficiency, abundance in natural resources, and non-toxicity. However, Si has a serious problem when it is used as a photoelectrode in aqueous electrolytes for solar to chemical conversion because it is easily oxidized at the surface and passivated. Since the solar to chemical conversion is regarded as a promising approach to low-cost solar energy conversion in Chapter 2, it is of key importance to find a way to stabilize Si without losing efficient photovoltaic characteristics.

A large number of studies have been made along this line.[3-5] He reported fairly long ago[6-10] that metal nano-dot coating was an effective way to get efficient n-Si electrodes, yielding very high open-circuit photovoltages (V_{oc}) of 0.62 to 0.64 V, considerably higher than those (about 0.59 V) for conventional p-n junction Si solar cells of a similar simple structure. This finding was of much interest, providing a new unique mechanism originating from metal nano-contact[7,8,10] to get efficient n-Si electrodes, but unfortunately the electrodes of this type showed no enough stability for long-term operation. Theoretically, it was expected[7,8] that the Si surface was stabilized by Pt dots at Pt-dotted parts and by passivating Si-oxide at naked parts, but actually gradual Si oxidation proceeded even beneath the Pt dots, thus leading to electrode degradation under long-term operation.

In Chapter 1 and 2, He has found that this instability problem in the metal nano-dot coating can be solved by combining it with surface alkylation developed by other workers.[11-17] A merit of the surface alkylation is the improvement of Si stability against the surface oxidation.[18,19] However, the surface alkylation itself has a detrimental action to retard interfacial electron transfer at the Si/electrolyte interface.[18,20-25] As reported in Chapter 1 and 2, the combination of the surface alkylation and metal nano-dot coating can provide a stable and efficient n-Si electrode because in this case the metal nano-dots act as an effective gate for

interfacial electron transfer. In fact, the detailed studies on the modification with various organic groups in Chapter 3 have shown that the surface alkylation at high coverage together with the coating with small Pt nano-dots really gives efficient and sufficiently stable n-Si electrodes.

In this chapter, he reports another interesting aspect of the Pt nano-dotted and surface-alkylated Si electrode in I_3^-/I^- redox electrolytes. The formation of Si-I bonds at non-modified (naked) Si surface sites induced adsorption of I^- ions, thus leading to a large negative shift in the flat-band potential (U_{fb}) of n-Si. This finding has provided a novel way to control the U_{fb} for n-Si and improve the solar cell characteristics.

Experimental

Single crystal n-Si (111) wafers of the resistivity of 1 ~ 5 Ω cm and the thickness of 825 ± 25 μm were donated by Osaka Tokushu-Gokin Co. Ltd. The wafers were first cleaned by the RCA cleaning method, and then immersed in 5% HF for 5 min and in 40% NH_4F for 15 min to get hydrogen (H)-terminated surfaces, as reported in previous chapters.

The surface alkylation was carried out by a method of photochlorination followed by a reaction with alkyl lithium, as reported in previous chapters. The H-terminated n-Si (111) was put in a saturated chlorobenzene solution of phosphorus pentachloride (PCl_5) and illuminated at 100°C by an ultrahigh pressure 500 W Hg lamp for 1 h. Then, the n-Si was refluxed in a solution of alkyl lithium. The alkyl lithium, solvent, and refluxing time, used in the present work, were 1.0 M CH_3Li, diethyl ether, 3 h; 2.6 M *n*-C_4H_9Li, *n*-hexane, 24 h; and 1.9 M *n*-$C_6H_{13}Li$, *n*-hexane, 24 h. All procedures were carried out under a dried argon atmosphere. The surface-alkylated Si wafers thus obtained were finally washed successively with diethyl ether, 2-propanol, and pure water.

Pt nano-dots were electrodeposited in 5 mM K_2PtCl_6 + 100 mM $LiClO_4$ on the beforehand surface-alkylated n-Si electrodes, using a platinum plate as the counter electrode and an Ag|AgCl(sat. KCl) electrode as the reference electrode, as reported in previous chapters. Ohmic contact with n-Si was obtained with indium-gallium alloy. The Pt deposition was carried out by stepping the potential from 0 V vs. Ag|AgCl(sat. KCl) to −1.0 V and then keeping it at −1.0 V, using a commercial set of a potentiostat, a potential programmer, and a recorder (Hokuto-Denko HSV-100). The electricity flowing across the Si surface was regulated to be 83 mC cm^{-2}, as measured with a digital coulomb meter (Nikko-Keisoku NDCM-3).

Photocurrent density (j) vs. potential (U), or solar cell characteristics, for Pt nano-dotted and surface-alkylated n-Si (111) electrodes were measured in aqueous I_3^-/I^- redox electrolytes, using a Pt plate as the counter electrode and a solar simulator (Kansai Kagaku Kikai

XES-502S, AM 1.5G 100 mW cm^{-2}) as the light source. The differential capacitances of the n-Si electrodes for Mott-Schottky plots were measured with an AC impedance electrochemical system (Solartron 1287 and 1260), using an Ag|AgCl(sat. KCl) electrode as the reference electrode and a Pt plate as the counter electrode. The applied AC voltage and frequency were 5 mV and 10 kHz, respectively. The U_{fb} shift by electrode illumination was investigated by illuminating the electrode weakly at about 3 mW cm^{-2} with a 50 W tungsten-halogen lamp. All chemicals were of reagent grade and used without further purification. Pure water of a resistivity of 18 MΩ cm^{-1}, obtained by a Milli-Q purification system, was used.

X-ray photoelectron spectroscopic (XPS) analysis of the Si surface was performed with a Shimadzu ESCA-1000 spectrometer using an MgKα line. Surface morphology was inspected with a Hitachi S-5000 high-resolution scanning electron microscope.

Results

First, let him describe the results of surface characterization for later discussion, though most of them were reported in previous chapters. The formation of atomically-flat H-terminated Si(111) surfaces by the HF and NH_4F etching, which were used as a substrate for the surface alkylation, was confirmed by observations of a clear step-terrace structure in AFM images[26-28] and a sharp strong FTIR peak at 2083.6 cm^{-1}, assigned to the stretching vibration of Si-H bonds at the (111) terrace, together with some weak peaks assigned to vibrations of Si-H and SiH_2 bonds at steps.[29,30] The methylation of the n-Si surface by the aforementioned treatment was, on the other hand, confirmed by observation of the XPS C-1s peak at 283.8 eV attributable to C in surface Si-CH_3 bonds,[31,32] distinguished from C 1s peaks due to contaminating hydrocarbons. A rough estimation of the surface coverage (θ) for CH_3 from the C-1s and Si-2p peaks, using the method of Himpsel et al.,[33] gave values of about 50 to 70 %, as reported.[34] As reported in Chapter 3, the modification with long alkyls was also confirmed by XPS analyses though the θ values were difficult to determine because of decreased intensities of the 283.8-eV peak. The AFM inspection revealed that the methylated n-Si surface showed a clear step and terrace structure similar to the H-terminated n-Si, indicating that the surface methylation gave little damage in the atomic-level structure of the Si surface.

As reported in previous chapters, the XPS analyses also revealed that the surface-alkylated n-Si showed almost no (or only a weak) Si-2p peak at around 104 eV, attributable to formation of SiO_2, even after the Pt deposition, clearly indicating that the surface alkyls effectively prevent the Si surface from oxidation. On the other hand, H-terminated n-Si showed, after the Pt deposition, a clear Si-2p peak at 104 eV, which was absent before the Pt deposition The effective surface oxidation in Pt-dotted (naked) n-Si in aqueous solutions is reported[35] to be due to hole injection into the Si valence band by dissolved oxygen with the deposited Pt as a catalyst.

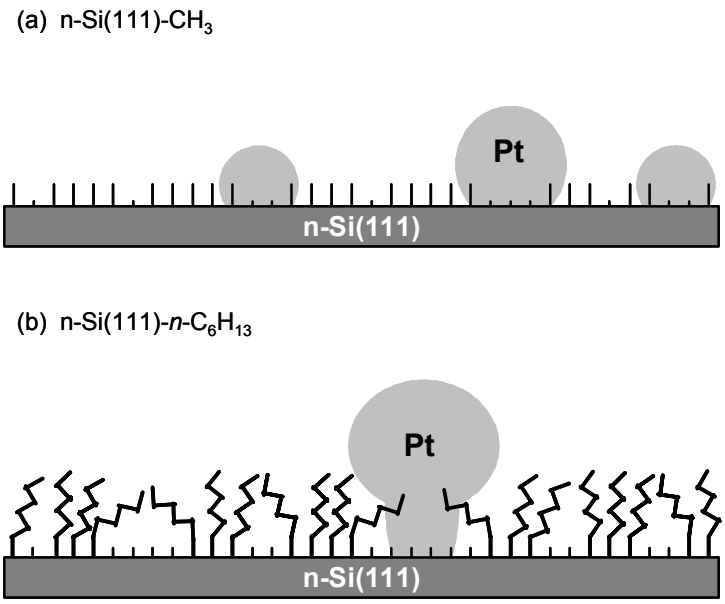

FIGURE 1 Schematic illustrations of structural models for the (a) surface-methylated and Pt-dotted and (b) surface hexylated and Pt-dotted n-Si(111) surfaces. Vertical short lines at the Si surface refer to non-alkylated Si-H (or Si-OH) sites, vertical long lines refer to CH_3-attached Si sites, and zigzag lines indicate *n*-C_6H_{13}.

Scanning electron micrographs (SEM's) of the surface-methylated and Pt nano-dotted n-Si showed that Pt particles with the average size of about 6 nm were deposited homogeneously all over the Si surface, similar to the case of H-terminated and Pt-dotted n-Si, though for the former n-Si, a small fraction of the Pt dots grew to large sizes of about 60 nm, as reported in previous chapters. The linear sweep voltammogram for the Pt electrodeposition (the Pt-deposition current measured under a negative potential sweep) on the surface-methylated n-Si was similar to that on the H-terminated n-Si, as reported in Chapter 3, indicating that the Pt dots for the surface-methylated n-Si was deposited on non-methylated (naked) parts of the Si surface, not on the methyl group. It will be reasonable that the surface-methylated Si surface with the coverage of about 50 to 70% has non-methylated nano-sized domains here and there, at which Pt can be deposited. For n-Si modified with long

alkyls such as n-C_4H_9 and n-C_6H_{13}, most of Pt dots grew to large sizes of 20 to 70 nm, with a much decreased density, as reported in Chapter 3. From these results, together with chronoamperograms for the Pt deposition, he proposed in Chapter 3 a structural model for the surface-alkylated and Pt-dotted n-Si(111) surfaces such as schematically shown in Figure 1.

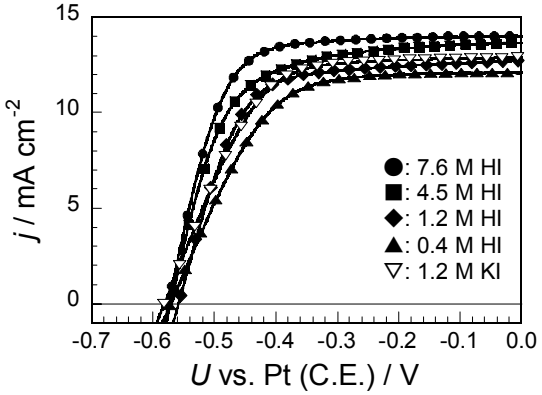

FIGURE 2 The *j*-*U* characteristics for n-Si(111)-CH_3/Pt under simulated solar (AM 1.5G, 100 mW cm^{-2}) illumination. The electrolyte: 0.05 M I_2 containing (●) 7.6 M HI, (■) 4.5 M HI, (◆) 1.2 M HI, (▲) 0.4 M HI, and (▽) 1.2 M KI. Note that not only the I^- concentration but also the solution pH change in these electrolytes. The scan rate: 0.05 V s^{-1}.

Now, let him describe results of photoelectrochemical measurements for the surface-methylated and Pt nano-dotted n-Si(111), hereafter abbreviated as n-Si(111)-CH_3/Pt. Figure 2 shows *j* vs. *U* (or solar cell) characteristics for n-Si(111)-CH_3/Pt in various aqueous I_3^-/I^- redox electrolytes, where the *U* is measured with respect to the Pt counter electrode (Pt(C.E.)). Interestingly, the *j*-*U* characteristics, in particular the V_{oc}, are nearly the same among the redox electrolytes, though the equilibrium redox potential $U_{eq}(I_3^-/I^-)$ and solution pH of the redox electrolytes are largely different from each other.

It is known[36-38] that the nearly constant V_{oc} for various redox couples with different

U_{eq}(redox) is observed when the Fermi level pinning via a surface state on a semiconductor occurs. In the present work, however, the nearly constant V_{oc} was observed only for the I_3^-/I^- redox couples with varied I^- concentrations and not for other redox couples. For example, a redox couple of $Ru(NH_3)_6^{2+}/Ru(NH_3)_6^{3+}$ (U_{eq} = 0.01 V vs. Ag|AgCl) gave a V_{oc} of 0.41 V, considerably smaller than that for the I_3^-/I^- redox couples. This implies that the constant V_{oc} in Figure 2 was not caused by the Fermi level pinning. This argument is supported also by the fact that the n-Si electrodes in Figure 2 yield high V_{oc}'s of about 0.58 V, fairly close to the highest V_{oc} for n-Si. If the n-Si had a high-density surface state that might induce the Fermi level pinning, such a high V_{oc} would never be obtained owing to efficient surface carrier recombination via the surface state.[7,8]

In order to investigate the reason for the constant V_{oc}, he then investigated the U_{fb} for n-Si(111)-CH_3/Pt in the same electrolytes as in Figure 2. Figure 3 shows some examples of Mott-Schottky plots, from which the U_{fb} could be determined as the potential at a cross point of the extrapolated straight line with the U axis.[20,39,40] He obtained, for reference, the Mott-Schottky plots for surface methylated but non-Pt-dotted n-Si (111) electrodes as well. Moreover, he obtained the plots not only in the dark but also under weak illumination (at a low intensity of about 3 mW cm^{-2}) in order to see the U_{fb} shift by illumination. Good straight lines were obtained in all cases, with the phase angles higher than 80°. The high phase angles assure that the Mott-Schottky plots obtained are reliable.[20,39,40] However, the slopes of the plots for the Pt dotted n-Si electrodes, in particular those in 7.6 M HI + 0.05 M I_2, were larger than those for the non-Pt-dotted ones (Figure 3). Repeated experiments gave the same U_{fb} values within experimental errors of ± 0.05 V, though the slope deviated to a small extent from experiment to experiment. The reason for the change in the slope is not clear at present. They might arise from a certain modulation of the Schottky barrier (or the space charge layer) of n-Si by the Pt nano-dot coating.

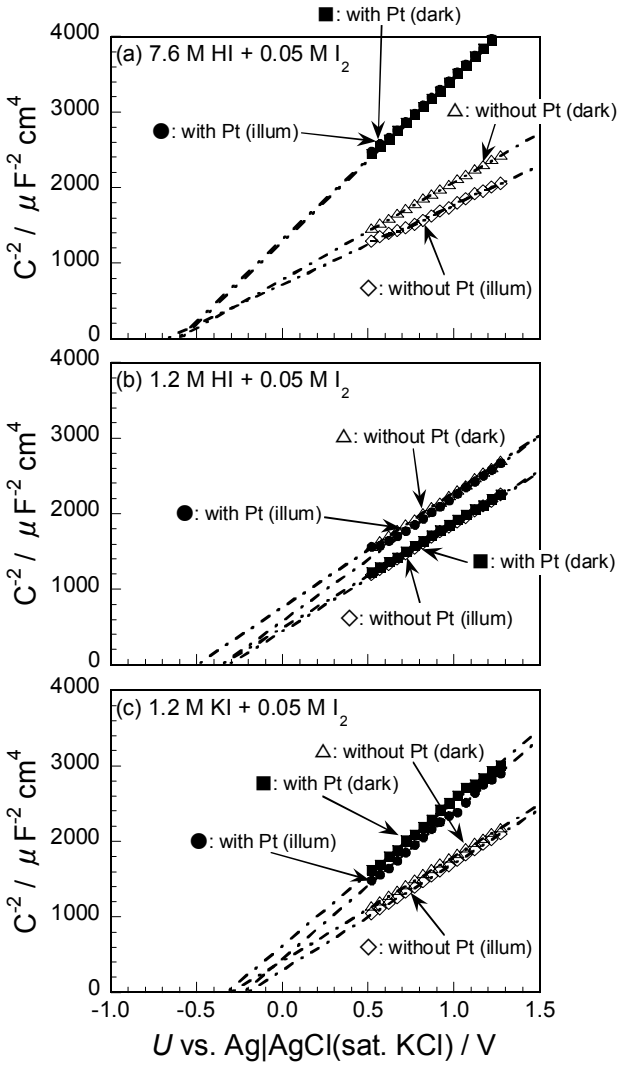

FIGURE 3 Mott-Schottky plots for n-Si(111)-CH_3 with and without Pt nano-dots, obtained in the dark and under weak illumination. The electrolyte: (a) 7.6 M HI + 0.05 M I_2, (b) 1.2 M HI + 0.05 M I_2, and (c) 1.2 M KI + 0.05 M I_2.

Table 1 summarizes the U_{fb} values thus obtained, together with the solar cell characteristics for n-Si(111)-CH_3/Pt in various I_3^-/I^- redox electrolytes. The $U_{eq}(I_3^-/I^-)$ values were determined from cyclic voltammograms with a Pt electrode in the I_3^-/I^- electrolytes. The U_{fb} in the dark, the photocurrent onset U_{on}, and the $U_{eq}(I_3^-/I^-)$ in Table 1 are also plotted in

Figure 4 as a function of the HI (I^-) concentration for easy comparison, together with the amount of adsorbed iodine on n-Si(111)-CH_3/Pt explained later. Figure 4 clearly indicates that the U_{fb} and U_{on} shift toward the negative with increasing the I^- concentration, nearly in parallel to the $U_{eq}(I_3^-/I^-)$. He can thus understand that this parallel shift of U_{fb} and $U_{eq}(I_3^-/I^-)$ is the reason for the nearly constant V_{oc}'s in Figure 2.

TABLE 1 The U_{fb} and solar cell characteristics for n-Si(111)-CH_3/Pt in various I_3^-/I^- redox electrolytes. The U_{fb} in parentheses are for n-Si with no Pt. All the electrolytes include 0.05 M I_2 though it is not indicated in the table. The experimental errors were ± 0.02 V for V_{oc}, U_{on}, and $U_{eq}(I_3^-/I^-)$: ±0.5 mA cm^{-2} for j_{sc}, and ± 0.05 V for U_{fb}.

Electrolyte	V_{oc} / V	j_{sc} / $mAcm^{-2}$	η / %	*F.F.*	$U_{eq}(I_3^-/I^-)$ vs. Ag|AgCl / V	U_{on} vs. Ag|AgCl / V	U_{fb} vs. Ag|AgCl / V	
							dark	illum
7.6M HI	0.58	14.0	5.67	0.701	0.08	-0.50	-0.63 (-0.64)	-0.64 (-0.53)
4.5M HI	0.57	13.7	5.06	0.645	0.19	-0.38	-0.54 (-0.58)	-0.53 (-0.58)
1.2M HI	0.56	12.7	4.70	0.661	0.35	-0.21	-0.38 (-0.45)	-0.39 (-0.35)
0.4M HI	0.57	12.1	4.16	0.601	0.39	-0.18	-0.38 (-0.34)	-0.30 (-0.22)
1.2M KI	0.58	12.9	4.64	0.618	0.34	-0.24	-0.24 (-0.45)	-0.45 (-0.31)

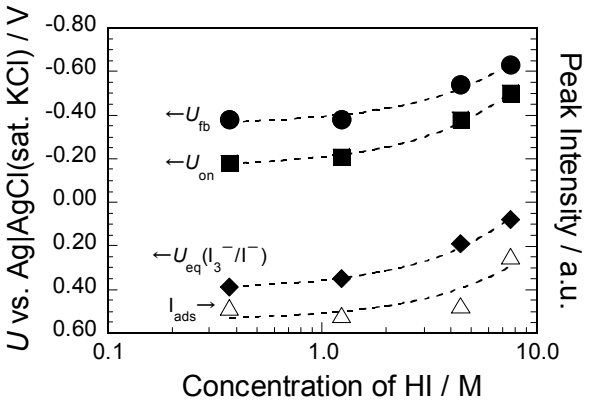

FIGURE 4 The (●) U_{fb} in the dark, (■) U_{on}, and (◆) $U_{eq}(I_3^-/I^-)$ for n-Si(111)-CH_3/Pt as a function of the HI concentration of the electrolytes (x M HI + 0.05 M I_2), together with the (△) XPS I $3d_{5/2}$ peak intensity for surface-methylated n-Si with no Pt, after immersion in the same electrolytes as above for 5 min in the dark.

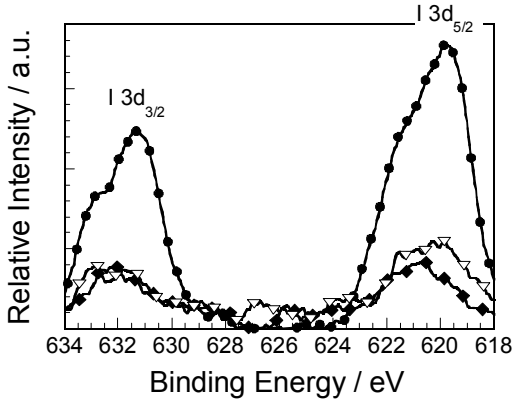

FIGURE 5 XPS I 3d peaks for methylated n-Si (111) with no Pt, after immersion in 0.05 M I_2 containing (●) 7.6 M HI, (◆) 1.2 M HI, and (▽) 1.2 M KI, for 5 min in the dark.

Why does the U_{fb} shift with the I^- concentration? In order to clarify the reason, he investigated the chemical composition of the n-Si surface by XPS. Figure 5 shows XPS I-3d peaks for surface methylated n-Si (111) with no Pt after immersion in the various I_3^-/I^- redox electrolytes. The n-Si with no Pt was chosen because for the Pt dotted n-Si, a considerable amount of iodine was adsorbed on the Pt dots and it was difficult to see the iodine adsorption on the Si surface. The immersion was carried out for 5 min in the dark, followed by sufficient washing with pure water. Two peaks assigned to I $3d_{3/2}$ and $3d_{5/2}$ were observed for all the electrolytes, suggesting that iodine was adsorbed at the n-Si surface. Unfortunately, as the reported I $3d_{5/2}$ peaks for I^- (KI) and I_2 are at nearly the same energy (619.2 eV) with almost no chemical shift, the XPS analyses could not give a definite conclusion on whether the surface iodine was in a form of Si-I or physisorbed I_2. However, the following facts strongly suggested that the surface iodine was in the form of Si-I: (1) The surface iodine was not removed even by thorough washing, and (2) the amount of the surface iodine decreased much with increasing the length of the surface alkyl chain, as mentioned later (Figure 8), which will be contrary to the behavior expected from the assumption of physisorbed I_2.

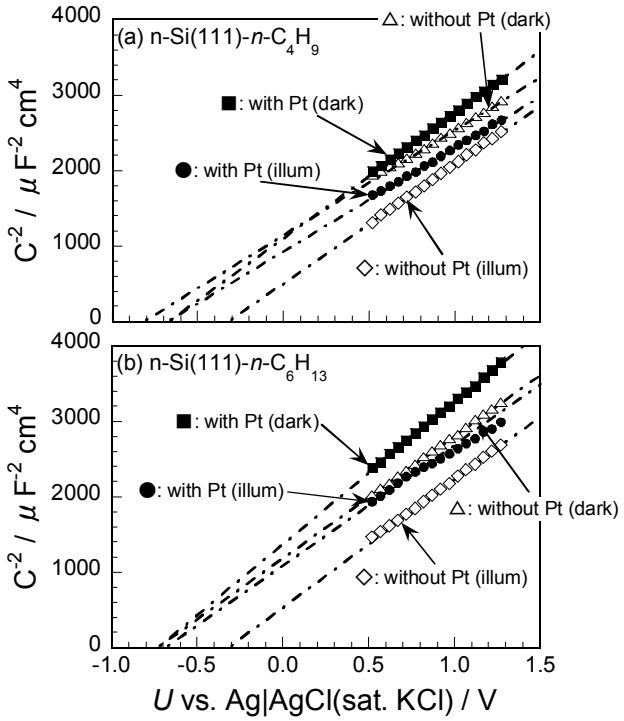

FIGURE 6 Mott-Schottky plots for n-Si(111)-*n*-C_4H_9/Pt and n-Si(111)-*n*-C_6H_{13}/Pt with and without Pt, obtained in the dark and under weak illumination. The electrolyte: 7.6 M HI + 0.05 M I_2.

The n-Si electrodes modified with Pt nano-dots and long-chain alkyls (R), abbreviated as n-Si(111)-R/Pt, gave essentially the same results as n-Si(111)-CH_3/Pt. Figure 6 shows, as some examples, the Mott-Schottky plots for n-Si(111)-*n*-C_4H_9/Pt and n-Si(111)-*n*-C_6H_{13}/Pt in 7.6 M HI + 0.05 M I_2. The plots for the n-Si electrodes with no Pt, and those under weak illumination were also included for reference, in the same way as in Figure 3. Figure 7 shows, also as some examples, the *j*-*U* (solar cell) characteristics for n-Si(111)-CH_3/Pt, n-Si(111)-*n*-C_4H_9/Pt, and n-Si(111)-*n*-C_6H_{13}/Pt in 7.6 M HI + 0.05 M I_2. Table 2 summarizes the U_{fb} and solar cell characteristics, similarly to Table 1. The U_{fb} shifts slightly toward the negative with increasing the alkyl chain length, though the V_{oc} remains nearly constant. It is to

be noted also that the U_{fb}'s for the n-C_4H_9- and n-C_6H_{13}-modified n-Si with no Pt (values in parentheses in Table 2) largely shift toward the positive by electrode illumination, in contrast to the cases with Pt nano-dots.

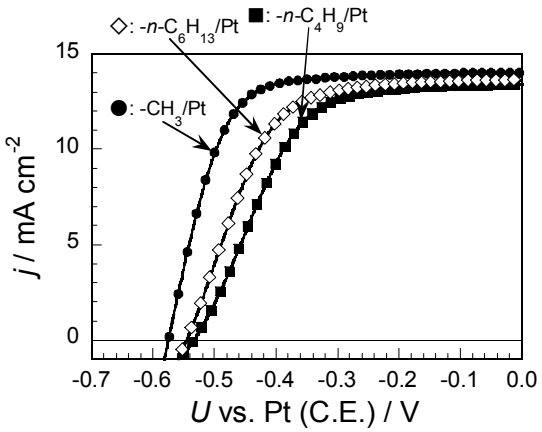

FIGURE 7 The *j*-*U* characteristics for (●) n-Si(111)-CH_3/Pt, (■) n-Si(111)-n-C_4H_9/Pt, and (◇) n-Si(111)-n-C_6H_{13}/Pt under simulated solar (AM 1.5G, 100 mW cm^{-2}) illumination. The electrolyte: 7.6 M HI + 0.05 M I_2. The scan rate was 0.05 V s^{-1}.

TABLE 2 The U_{fb} and solar cell characteristics for n-Si(111)-R/Pt (R = CH_3, n-C_4H_9, and n-C_6H_{13}) in 7.6 M HI + 0.05 M I_2, represented in the same way as in Table 1. The U_{fb} in parentheses are for n-Si with no Pt. The experimental errors were the same as in Table 1.

Alkyl group	V_{oc} / V	j_{sc} / mAcm^{-2}	U_{on} vs. Ag|AgCl / V	U_{fb} vs. Ag|AgCl / V dark	illum
CH_3	0.576	14.03	-0.50	-0.63 (-0.64)	-0.64 (-0.53)
n-C_4H_9	0.535	13.41	-0.45	-0.70 (-0.85)	-0.71 (-0.36)
n-C_6H_{13}	0.546	13.63	-0.47	-0.77 (-0.77)	-0.72 (-0.35)

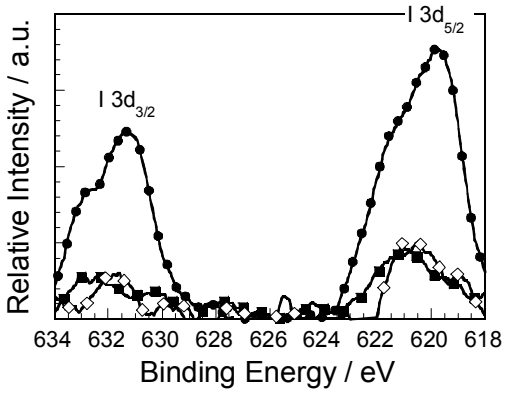

FIGURE 8 XPS I 3d peaks for (●) CH_3-, (■) *n*-C_4H_9-, and (◇) *n*-C_6H_{13}-modified n-Si with no Pt, after immersion in 7.6 M HI + 0.05 M I_2 for 5 min in the dark.

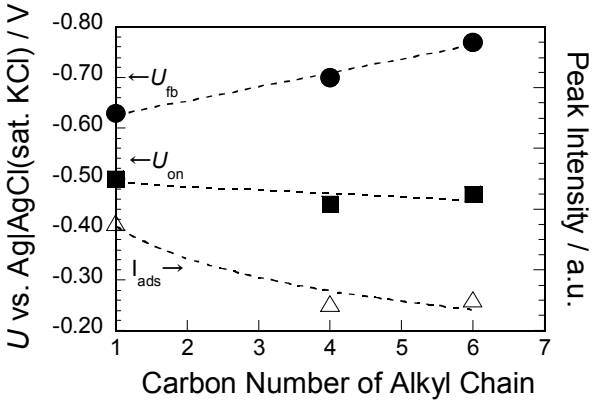

FIGURE 9 The (●) U_{fb} in the dark and (■) U_{on} for n-Si(111)-CH_3/Pt, n-Si(111)-*n*-C_4H_9/Pt, and n-Si(111)-*n*-C_6H_{13}/Pt in 7.6 M HI + 0.05 M I_2 as a function of the carbon number of the modifying alkyl chains, together with the (△) XPS I $3d_{5/2}$ peak intensity for CH_3-, *n*-C_4H_9-, and *n*-C_6H_{13}-modified n-Si with no Pt after immersion in 7.6 M HI + 0.05 M I_2 for 5 min in the dark.

Figure 8 shows the XPS I 3d peaks for the CH_3-, *n*-C_4H_9-, and *n*-C_6H_{13}-modified n-Si (111) with no Pt, after immersion in 7.6 M HI + 0.05 M I_2 for 5 min in the dark. The n-Si with no Pt was chosen to see the iodine adsorption on Si as separated from that on Pt, as mentioned earlier. The results indicate that iodine is adsorbed also on the *n*-C_4H_9 and *n*-C_6H_{13}-modified n-Si, though the amount is considerably smaller than the case of CH_3-modified n-Si. Figure 9 shows the U_{fb} in the dark and the U_{on} for n-Si(111)-CH_3/Pt, n-Si(111)-*n*-C_4H_9/Pt, and n-Si(111)-*n*-C_6H_{13}/Pt in 7.6 M HI + 0.05 M I_2 as a function of the alkyl-chain length, together with the XPS I $3d_{5/2}$ peak intensity for alkylated n-Si with no Pt after immersion in 7.6 M HI + 0.05 M I_2 for 5 min in the dark.

Discussion

The experimental results described in the preceding section show that the surface alkylated and Pt nano-dotted n-Si(111) electrodes yield efficient solar cell characteristics in the I_3^-/I^- electrolyte, as reported in previous chapters, though they show a slight dependence on the alkyl chain length. A remarkable point of the present work is that the V_{oc} for the surface-methylated and Pt nano-dotted n-Si electrode hardly depended on the $U_{eq}(I_3^-/I^-)$ of the electrolytes (Figure 2), or in other words, the U_{fb} for this n-Si electrode shifted nearly in parallel to the $U_{eq}(I_3^-/I^-)$ (Figure 4). He argued in the preceding section that the nearly constant V_{oc} [or the parallel shift of U_{fb} with $U_{eq}(I_3^-/I^-)$] could not be attributed to the Fermi level pinning via a surface state. Thus, the remaining problem is why the V_{oc} is kept constant or why the U_{fb} shifts nearly in parallel to the $U_{eq}(I_3^-/I^-)$. Let him first consider this problem.

The U_{fb} is theoretically determined[3-5] by the electron affinity of a semiconductor and a surface potential arising from interfacial (or Helmholtz) double layers due to ion adsorption, surface bond dipoles, etc., and is in general independent of the equilibrium redox potential of the redox electrolyte if the Fermi level pinning is absent. Thus, the V_{oc} in general changes in proportion to the change in the equilibrium redox potential of the redox electrolyte. In fact, the Pt nano-dotted n-Si showed a linear relation between the change in the V_{oc} and that in the equilibrium redox potential of the electrolyte,[7,8] indicating that the above argument holds for this type of n-Si electrodes.

One might point out that the oxidation of the Si surface could be responsible for the U_{fb} shifts. This possibility is, however, excluded because the XPS analyses show almost no formation of a surface oxide layer for the surface methylated and Pt dotted n-Si, as mentioned earlier, contrary to the case of non-alkylated (H-terminated) and Pt dotted n-Si. Besides, the surface oxidation, if any, cannot explain the U_{fb} shifts because the observed U_{fb} is independent of the solution pH (Figure 4). If ionic charges on the surface oxide were responsible for the U_{fb}

shift, the U_{fb} should shift to the positive with decreasing pH,[3-5,39] contrary to the experimental results (Figure 4).

One might point out also that the adsorption of iodine on the Pt particles might affect the U_{fb}. However, this possibility is also excluded because the Pt particles in the present work are in contact with the I_3^-/I^- redox electrolyte, and therefore the Fermi level of Pt is entirely regulated by the redox level of the redox couple via electron exchange equilibrium, irrespective of surface chemistry of Pt. Namely, even if iodine or iodide is adsorbed on Pt, the Fermi level of Pt is kept to equal the redox level of the redox electrolyte. Moreover, a change in the Fermi level of Pt particles does not affect the U_{fb} of n-Si if the particle size is very small, i.e. about 5 nm, as discussed in detail in previous papers.[7,8]

He can show below that the U_{fb} shift can be explained reasonably by taking into account the iodine adsorption at the Si surface. The upper part of Figure 1 schematically illustrates a structural model for the surface-methylated and Pt nano-dotted n-Si(111), derived through detailed studies on it in Chapter 3. The main features are, (1) the surface coverage (θ_{CH3}) for CH_3 is about 50 to 70%, and (2) the deposition of the Pt particles occurs at non-alkylated Si sites, in particular, at a part of assemblies of non-alkylated Si sites with appropriately large areas. The latter argument is based on a consideration that an anionic reactant, $[PtCl_6]^{2-}$, in the Pt deposition has a large hydration sphere and thus the Pt deposition will occur only at a part of assemblies of non-alkylated Si sites with appropriately large areas, as reported in Chapter 3. This implies that a number of isolated Si-H (or Si-OH) sites remains at the Si surface, as illustrated in Figure 1. Accordingly, when the surface-methylated and Pt nano-dotted n-Si(111) is immersed in an I_3^-/I^- redox electrolyte, I^- ions will be adsorbed at the Si-H (or Si-OH) sites, as reported in a previous paper[41], resulting in surface Si-I bonds,

$$\text{Si-H (or Si-OH)} + I^- + H^+ \rightarrow \text{Si-I} + H_2 \text{ (or } H_2O) \qquad (1)$$

The bond energy for Si-H (or Si-OH) is larger than that for Si-I, but this reaction will be thermodynamically feasible because stable molecules with strong bonds such as H_2 or H_2O are produced as a product. The formation of Si-I bonds is supported also by the observation of the XPS I-3d peaks, assignable to the Si-I bonds, at the n-Si surface after its immersion in the I_3^-/I^- electrolytes, as mentioned in the preceding section (Figures 5 and 8).

Based on this model, he can then assume that I^- ions in the electrolytes are further adsorbed on the Si-I bonds, forming an Si-I···I^- complex at the surface.

$$\text{Si-I} + I^- \rightarrow \text{Si-I}\cdots I^- \qquad (2)$$

This assumption is reasonable because it is well known that an I_2 molecule forms a (Mulliken's charge-transfer) complex with an I^- ion, resulting in an I_3^- ion.

$$\text{I-I} + I^- \rightarrow \text{I-I}\cdots I^- \qquad (3)$$

The surface complex, Si-I···I^-, in equation (2) can be regarded as of the same electronic nature as the I-I···I^- complex.

The formation of the Si-I···I^- complex gives rise to negative charges at the Si surface, which are responsible for the negative shift in the U_{fb}. This concept is essentially the same as that for well-known negative shifts in the U_{fb} with increasing the solution pH for metal-oxide semiconductors such as n-TiO_2 and n-ZnO, which are attributed to either desorption of H^+ ions from the surface or adsorption of OH^- ions to the surface. The potential drop ($\Delta\phi_H$) at the Helmholtz layer (defined as the potential at the surface vs. the electrolyte solution), which leads to the U_{fb} shift, is calculated by assuming an ionic adsorption equilibrium for equation (2), in which the electrochemical potentials are equal on the right- and left-hand sides

$$\mu_{\text{Si-I}} + \mu_{\text{I}^-} = \mu_{\text{Si-I}\cdot\text{I}^-} - q\Delta\phi_{\text{H}} \quad (4)$$

where μ_α is the chemical potential for species α and q is the elementary charge. Equation (4) can be rewritten by using the surface coverage ($\theta_{\text{Si-I}}$) for Si-I and that ($\theta_{\text{Si-I}\cdot\text{I}^-}$) for Si-I···I$^-$, and the concentration (C_{I^-}) for I$^-$ ions in the electrolyte,

$$\Delta\phi_{\text{H}} = (\mu_{\text{Si-I}\cdot\text{I}^-}{}^0 - \mu_{\text{Si-I}}{}^0 - \mu_{\text{I}^-}{}^0)/q + (kT/q)\ln(\gamma_{\text{Si-I}\cdot\text{I}^-}\theta_{\text{Si-I}\cdot\text{I}^-}/\gamma_{\text{Si-I}}\theta_{\text{Si-I}}) - (kT/q)\ln(\gamma_{\text{CI}^-}C_{\text{I}^-}) \quad (5)$$

where the superscript "0" means the standard state and γ_α is the activity coefficient for species α. Equation (5) implies that $\Delta\phi_{\text{H}}$, i.e. the U_{fb}, changes in proportion to $-(kT/q)\ln(\gamma_{\text{CI}^-}C_{\text{I}^-})$ if the term, $\ln(\gamma_{\text{Si-I}\cdot\text{I}^-}\theta_{\text{Si-I}\cdot\text{I}^-}/\gamma_{\text{Si-I}}\theta_{\text{Si-I}})$, is kept nearly constant for changes in $\theta_{\text{Si-I}\cdot\text{I}^-}$ and $\theta_{\text{Si-I}}$. This condition holds as far as the $\theta_{\text{Si-I}}$ and $\theta_{\text{Si-I}\cdot\text{I}^-}$ are not near zero or one. On the other hand, the $U_{\text{eq}}(\text{I}_3^-/\text{I}^-)$ also shifts in proportion to $-(kT/q)\ln(\gamma_{\text{CI}^-}C_{\text{I}^-})$ according to Nernst equation. Accordingly, the U_{fb} shifts with increasing the I$^-$ concentration in parallel to the $U_{\text{eq}}(\text{I}_3^-/\text{I}^-)$, in agreement with the observed behavior for the U_{fb} and $U_{\text{eq}}(\text{I}_3^-/\text{I}^-)$ (Figure 4).

From the above arguments, one may feel it strange that no dependence of the U_{fb} on the I$^-$ concentration has been observed for the H-terminated and Pt-dotted n-Si, which would have a high density of Si-H sites. This is because the H-terminated n-Si surface is immediately oxidized when Pt is deposited, by the hole injection via molecular oxygen in air as an oxidant, with the Pt particles acting as a catalyst. At the oxidized Si surface, the I$^-$ adsorption (or Si-I formation) can no longer occur.

Figure 9 shows that the U_{fb} for the Pt nano-dotted and long-alkyl modified n-Si (111) shifts slightly toward the negative with increasing the alkyl chain length, though the U_{on} or V_{oc}

remains nearly constant. The negative U_{fb} shift in this case will also be explained within a framework of discussion made above, because the long-alkyl modified n-Si shows the presence of adsorbed iodine (Figure 8). A possible explanation might be given by assuming either that the standard chemical potentials, $\mu_{Si\text{-}I\cdot I-}{}^{0}$ and/or $\mu_{Si\text{-}I}{}^{0}$, change with increasing the alkyl chain length, or that the $\theta_{Si\text{-}I}$ and/or $\theta_{Si\text{-}I\cdot I-}$ are coming near zero for the long-alkyl modified n-Si, as is expected from Figure 8, and thus the term, ln ($\gamma_{Si\text{-}I\cdot I-}\theta_{Si\text{-}I\cdot I-}/\gamma_{Si\text{-}I}\theta_{Si\text{-}I}$), can no longer be regarded to be nearly constant for the changes in $\theta_{Si\text{-}I\cdot I-}$ and $\theta_{Si\text{-}I}$. The nearly constant U_{on} or V_{oc}, in spite of the negative U_{fb} shifts, can be attributed to the increase in the size of the Pt nano-dots, or the increase in the area of direct Pt-Si contact, for the long-alkyl modified n-Si, as reported in Chapter 3. The group he belongs to discussed in detail previously[10,11] that the increase in the area of the direct Pt-Si contact led to the decrease in the effective barrier height for the n-Si electrodes and hence the decrease in the V_{oc}. It is likely that the negative U_{fb} shift with increasing alkyl chain length is nearly compensated by the decrease in the effective barrier height due to the increase in the Pt-particles size.

He has also mentioned in the preceding section that the U_{fb}'s for the n-C_4H_9- and n-C_6H_{13}-modified n-Si with no Pt largely shift (by about 0.3 V) toward the positive by electrode illumination, in contrast to the cases of alkylated n-Si with Pt nano-dots. This result can be explained by taking into account that the surface alkyl group has a detrimental effect for interfacial electron transfer reactions, as reported,[18,20-25] and thus photogenerated holes for the long-alkyl modified n-Si with no Pt are accumulated at the Si surface, leading to the positive shift in the U_{fb}. For the Pt dotted electrodes, on the other hand, the Pt dots act as an efficient catalyst (or gate) for the interfacial electron transfer, thus leading to no accumulation of photogenerated holes at the surface and hence no U_{fb} shift. The results clearly indicate the important role of the Pt nano-dots in obtaining efficient n-Si electrodes.

In conclusion, the present work has revealed that the Pt nano-dotted and surface

methylated n-Si (111) electrodes yield nearly the same V_{oc} among various I^-/I_3^- redox electrolytes with different $U_{eq}(I_3^-/I^-)$ owing to the fact that the U_{fb} shifts toward the negative with increasing the I^- concentration, in parallel to $U_{eq}(I_3^-/I^-)$. The negative U_{fb} shifts are explained in terms of I^- adsorption in the form of Si-I···I^-. Besides, the U_{fb} measurements in the dark and under illumination have clearly indicated that the Pt nano-dots act as an efficient gate for interfacial electron transfer and prevent the positive shift in the U_{fb} under illumination (or the decrease in the V_{oc}). The results are of much interest, indicating that a combination of the surface anionic adsorption with the surface alkylation and the Pt nano-dot coating is a novel effective way to obtain efficient and stable n-Si electrodes.

References

(1) Sze, S. M. *Semiconductor Devices: Physics and Technology*, 2nd. ed.; John Wiley & Sons: New York, 2002; pp 282 ff.

(2) Center for Photovoltaic Engineering, UNSW (The University of New South Wales) Home Page. http://www.pv.unsw.edu.au/Research/scet.asp (accessed Jan 2006).

(3) Pleskov, Y. V.; Gurevich, Y. Y.; Bartlett, P. N. *Semiconductor Photoelectrochemistry*; Consultants Bureau: New York, 1986.

(4) Nozik, A. J.; Memming, R. *J. Phys. Chem.* **1996**, *100*, 13061.

(5) Nakato, Y. Photoelectrochemical Cells. In *Wiley Encyclopedia of Electrical and Electronics Engineering Online (www.interscience.wiley.com)*; Webster, J., Ed.; John Wiley & Sons, Inc., 2000.

(6) Nakato, Y.; Yano, H.; Tsubomura, H. *Chem. Lett.* **1986**, 987.

(7) Nakato, Y.; Ueda, K.; Yano, H.; Tsubomura, H. *J. Phys. Chem.* **1988**, *92*, 2316.

(8) Nakato, Y.; Tsubomura, H. *Electrochim. Acta* **1992**, *37*, 897.

(9) Jia, J. G.; Fujitani, M.; Yae, S.; Nakato, Y. *Electrochim. Acta* **1997**, *42*, 431.

(10) Ishida, M.; Morisawa, K.; Hinogami, R.; Jia, J. G.; Yae, S.; Nakato, Y. *Z. Phys. Chem.* **1999**, *212*, 99.

(11) Linford, M. R.; Chidsey, C. E. D. *J. Am. Chem. Soc.* **1993**, *115*, 12631.

(12) Linford, M. R.; Fenter, P.; Eisenberger, P. M.; Chidsey, C. E. D. *J. Am. Chem. Soc.* **1995**, *117*, 3145.

(13) Bansal, A.; Li, X. L.; Lauermann, I.; Lewis, N. S.; Yi, S. I.; Weinberg, W. H. *J. Am. Chem. Soc.* **1996**, *118*, 7225.

(14) Buriak, J. M. *Chem. Commun.* **1999**, 1051.

(15) Okubo, T.; Tsuchiya, H.; Sadakata, M.; Yasuda, T.; Tanaka, K. *Appl. Surf. Sci.* **2001**, *171*, 252.

(16) Wayner, D. D. M.; Wolkow, R. A. *J. Chem. Soc., Perkin Trans. 2* **2002**, 23.

(17) Buriak, J. M. *Chem. Rev.* **2002**, *102*, 1271.

(18) Bansal, A.; Lewis, N. S. *J. Phys. Chem. B* **1998**, *102*, 4058.

(19) Royea, W. J.; Juang, A.; Lewis, N. S. *Appl. Phys. Lett.* **2000**, *77*, 1988.

(20) Bansal, A.; Lewis, N. S. *J. Phys. Chem. B* **1998**, *102*, 1067.

(21) Yu, H. Z.; Boukherroub, R.; Morin, S.; Wayner, D. D. M. *Electrochem. Commun.* **2000**, *2*, 562.

(22) Barrelet, C. J.; Robinson, D. B.; Cheng, J.; Hunt, T. P.; Quate, C. F.; Chidsey, C. E. D. *Langmuir* **2001**, *17*, 3460.

(23) Cheng, J.; Robinson, D. B.; Cicero, R. L.; Eberspacher, T.; Barrelet, C. J.; Chidsey, C. E. D. *J. Phys. Chem. B* **2001**, *105*, 10900.

(24) Zhao, J. W.; Uosaki, K. *Appl. Phys. Lett.* **2003**, *83*, 2034.

(25) Niwa, D.; Inoue, T.; Fukunaga, H.; Akasaka, T.; Yamada, T.; Homma, T.; Osaka, T. *Chem. Lett.* **2004**, *33*, 284.

(26) Imanishi, A.; Nagai, T.; Nakato, Y. *J. Phys. Chem. B* **2004**, *108*, 21.

(27) Imanishi, A.; Hayashi, T.; Nakato, Y. *Langmuir* **2004**, *20*, 4604.

(28) Imanishi, A.; Suzuki, M.; Nakato, Y. *Trans. Mater. Res. Soc. Jpn.* **2004**, *29*, 3223.

(29) Zhou, X. W.; Ishida, M.; Imanishi, A.; Nakato, Y. *Electrochim. Acta* **2000**, *45*, 4655.

(30) Zhou, X. W.; Ishida, M.; Imanishi, A.; Nakato, Y. *J. Phys. Chem. B* **2001**, *105*, 156.

(31) Liu, H. B.; Hamers, R. J. *Surf. Sci.* **1998**, *416*, 354.

(32) Terry, J.; Linford, M. R.; Wigren, C.; Cao, R. Y.; Pianetta, P.; Chidsey, C. E. D. *J. Appl. Phys.* **1999**, *85*, 213.

(33) Himpsel, F. J.; McFeely, F. R.; Talebibrahimi, A.; Yarmoff, J. A.; Hollinger, G. *Phys. Rev. B* **1988**, *38*, 6084.

(34) Cicero, R. L.; Linford, M. R.; Chidsey, C. E. D. *Langmuir* **2000**, *16*, 5688.

(35) Yae, S.; Kawamoto, Y.; Tanaka, H.; Fukumuro, N.; Matsuda, H. *Electrochem. Commun.* **2003**, *5*, 632.

(36) Bardeen, J. *Phys. Rev.* **1947**, *71*, 717.

(37) Bard, A. J.; Bocarsly, A. B.; Fan, F. R. F.; Walton, E. G.; Wrighton, M. S. *J. Am. Chem. Soc.* **1980**, *102*, 3671.

(38) Nakato, Y.; Tsumura, A.; Tsubomura, H. *J. Electrochem. Soc.* **1981**, *128*, 1300.

(39) Morrison, S. R. *Electrochemistry at Semiconductor and Oxidized Metal Electrodes*; Plenum Press: New York, 1980.

(40) Bard, A. J.; Faulkner, L. R. *Electrochemical Methods: Fundamentals and Applications*, 2nd. ed.; John Wiley & Sons: New York, 2001; pp 368 ff and 736 ff.

(41) Fujitani, M.; Hinogami, R.; Jia, J. G.; Ishida, M.; Morisawa, K.; Yae, S.; Nakato, Y. *Chem. Lett.* **1997**, 1041.

General Conclusion

Although the realization of the solar energy conversion has been strongly desired in the present societies owing to its clean nature, recent studies in this field still have serious problems, in particular, in the lowering of the fabrication cost. In the present work, the author has adopted an approach of solar to chemical conversion by use of a semiconductor/electrolyte junction in view of its large merits in the cost lowering, and studied the surface alkylated and Pt nano-dotted n-Si electrodes for the purpose of obtaining the efficient and stable electrodes. The main strategy has been to combine the method of surface alkylation for the stability and the method of metal nano-dot coating for the high efficiency. The author has finally succeeded in demonstrating that this strategy really provides highly efficient and stable n-Si electrodes.

First, the author has succeeded in demonstrating that the surface methylated n-Si (111) electrodes with Pt nano-dots give efficient and stable photocurrent vs. potential characteristics in an aqueous HBr/Br_2 redox electrolyte of a highly corrosive nature for more than 6 h (Chapter 1). He has shown that the surface alkyl group effectively prevents the oxidation at the Si surface and that the surface Pt nano-dots act as an effective catalyst (or gates) for interfacial electron transfer, thus effectively overcoming the demerit of the surface alkylation to retard interfacial electron transfer. The results have shown that the surface alkylated and Pt nano-dotted n-Si (111) electrode is a new-type ideal semiconductor electrode for solar energy conversion.

The author has also succeeded in showing that the surface methylated and Pt nano-dotted n-Si (111) electrode can successfully be used for photodecomposition of hydrogen iodide into hydrogen and iodine in an electrochemical cell with no external bias (Chapter 2). Actual experiments have shown that this system yields a solar to chemical conversion efficiency (ϕ^{s}_{chem}) of 7.4 %, which is the highest ever reported, apart from high values reported

for MBE-made expensive high-quality composite multiplayer semiconductor electrodes. The success is important in that it has opened a new way of cost lowering for solar energy conversion.

Further studies on the Pt nano-dotted and surface-alkylated n-Si (111) electrodes in the I_3^-/I^- redox electrolyte have shown that the surface alkylation gives high overvoltages for the Pt electrodeposition and leads to growth of large-sized Pt particles (Chapter 3). This tendency has become more prominent with increasing the surface alkyl chain length. The photovoltaic behavior and stability for the surface alkylated n-Si electrodes were improved much by the Pt-dot coating, but became somewhat inferior with increasing the alkyl chain length. These results have suggested the importance of mutually regulated attachments of surface alkyl groups and Pt nano-dots as a research subject in the future.

The author has also revealed that the flat-band potentials (U_{fb}) for the Pt nano-dotted and surface alkylated n-Si (111) electrodes in the I_3^-/I^- redox electrolytes shift toward the negative with increasing the I^- concentration, in parallel to the equilibrium redox potential $U_{eq}(I_3^-/I^-)$, and thus the V_{oc} is kept nearly constant among the I_3^-/I^- redox electrolytes with different $U_{eq}(I_3^-/I^-)$ and different pH. The U_{fb} shift is explained in terms of formation of a surface adsorption complex in the form of Si-I···I^-, which induces negative charges at the surface for the negative shift in U_{fb}. This result is of much interest, not only from the point of view of the increase in V_{oc} but also from the regulation of the U_{fb} of the n-Si electrodes.

In short, the present work has established that a combination of surface alkylation and metal nano-dot coating is an effective way to obtain a highly efficient and stable n-Si electrode for solar energy conversion. As the Si is the most important and suitable semiconductor for solar energy conversion, the present success in utilizing it as a photoelectrode for solar to chemical conversion is of key importance in that it has opened a new way of cost lowering in the solar energy conversion.

Acknowledgements

First of all, the author would like to express his sincerest gratitude to Professor Yoshihiro Nakato for his continuous instruction, advice, guidance, and encouragement.

The author also would like to express his sincerest gratitude to Professors Michio Matsumura and Hiroshi Miyasaka for their useful comments and suggestions. He would like to express his deep thanks to Professor Kei Murakoshi (Hokkaido University), Associate Professor Akihito Imanishi, and Dr. Shuji Nakanishi for their invaluable advice and support in this laboratory.

The author is particularly indebted to sincerest advice for this dissertation: Associate Professor Shinji Yae (University of Hyogo) on photoelectrochemistry; Professor Kazushi Mashima and Dr. Masato Ohashi (Mashima Laboratory) on organometallic chemistry; Professor Shoko Yamazaki and Dr. Yang Liu (Nara University of Education) on organic chemistry.

The author would like to express his sincerest gratitude to Professor Susumu Kuwabata, Professor Tsukasa Torimoto (Nagoya University), Dr. Daisuke Oyamatsu, and Dr. Hirokazu Munakata for continuous advice, guidance, and encouragement in Kuwabata Laboratory (Division of Applied Chemistry, Graduate School of Engineering).

The author wishes to thank his collaborators: Dr. Ken-ichi Okazaki, Dr. Ryuhei Nakamura, Mr. Keisuke Nakato, Mr. Takeshi Murata, Ms. Haruka Yamasaki, and Mr. Naoaki Kato. Furthermore, he would like to express his sincerest gratitude to Ms. Noriko Wada, Ms. Yayoi Ito, and Ms. Mariko Yamaoka for their continuous encouragement and support.

Finally, the author would like to express his inestimably deep thanks to his parents, grandfather, and beloved grandmother who has gone to heaven on 21st. Jan.

January, 2006

Susumu Takabayashi